VYSOKÉ UČENÍ TECHNICKÉ V BRNĚ
BRNO UNIVERSITY OF TECHNOLOGY

FAKULTA STROJNÍHO INŽENÝRSTVÍ
FACULTY OF MECHANICAL ENGINEERING

ÚSTAV FYZIKÁLNÍHO INŽENÝRSTVÍ
INSTITUTE OF PHYSICAL ENGINEERING

TEMPLATE ASSISTED ELECTRODEPOSITION OF MULTILAYER NANOSTRUCTURES

DIPLOMOVÁ PRÁCE
MASTER'S THESIS

AUTOR PRÁCE Bc. TOMÁŠ LEDNICKÝ
AUTHOR

BRNO 2014

VYSOKÉ UČENÍ TECHNICKÉ V BRNĚ
BRNO UNIVERSITY OF TECHNOLOGY

FAKULTA STROJNÍHO INŽENÝRSTVÍ
FACULTY OF MECHANICAL ENGINEERING

ÚSTAV FYZIKÁLNÍHO INŽENÝRSTVÍ
INSTITUTE OF PHYSICAL ENGINEERING

TEMPLATE ASSISTED ELECTRODEPOSITION OF MULTILAYER NANOSTRUCTURES

PŘÍPRAVA VÍCEVRSTEVNÝCH STRUKTUR POMOCÍ ELEKTRODEPOZICE V ŠABLONÁCH

DIPLOMOVÁ PRÁCE
MASTER'S THESIS

AUTOR PRÁCE — Bc. TOMÁŠ LEDNICKÝ
AUTHOR

VEDOUCÍ PRÁCE — Ing. JAN ČECHAL, Ph.D.
SUPERVISOR

BRNO 2014

Vysoké učení technické v Brně, Fakulta strojního inženýrství

Ústav fyzikálního inženýrství
Akademický rok: 2013/14

ZADÁNÍ DIPLOMOVÉ PRÁCE

student(ka): Bc. Tomáš Lednický

který/která studuje v **magisterském studijním programu**

obor: **Fyzikální inženýrství a nanotechnologie (3901T043)**

Ředitel ústavu Vám v souladu se zákonem č.111/1998 o vysokých školách a se Studijním a zkušebním řádem VUT v Brně určuje následující téma diplomové práce:

Příprava vícevrstevných struktur pomocí elektrodepozice v šablonách

v anglickém jazyce:

Template assisted electrodeposition of multilayer nanostructures

Stručná charakteristika problematiky úkolu:

Experimentální práce věnovaná metodám přípravy vícevrstevných materiálů (např. Au/polymer/Au) pomocí elektrodepozice v šablonách. Jako šablony budou použity vrstvy porézního Al2O3.

Cíle diplomové práce:

1. Stručně popište základní principy elektrodepozice a základní vlastnosti šablon.
2. Připravte šablony tvořené porézním Al2O3.
3. Studujte vlastnosti připravených struktur v závislosti na parametrech depozice. Realizujte strukturu tvořenou trojvrstvou Au/Polymer/Au

Seznam odborné literatury:

[1] C. Dupas, P. Houdy, M. Lahmani: Nanoscience, Springer–Verlag, Heidelberg 2007.
[2] Články v odborných a vědeckých časopisech.

Vedoucí diplomové práce:Ing. Jan Čechal, Ph.D.

Termín odevzdání diplomové práce je stanoven časovým plánem akademického roku 2013/14.

V Brně, dne 9.12.2013

L.S.

VYSOKÉ UČENÍ TECHNICKÉ V BRNĚ FAKULTA STROJNÍHO INŽENÝRSTVÍ DĚKANÁT

prof. RNDr. Tomáš Šikola, CSc.
Ředitel ústavu

prof. RNDr. Miroslav Doupovec, CSc., dr. h. c.
Děkan

ABSTRACT

This diploma thesis is focused on the fabrication of Au-PANI-Au nanowires. The fabrication of nanowires based on the electrochemical deposition of various metal and polymerization of polyaniline within porous templates is presented. Preparation of porous anodic alumina templates by the anodization of aluminium is described in detail. The theoretical part covers the basics of the electrochemistry and it provides a broad overview of the porous anodic alumina.

KEYWORDS

anodization, electrochemical deposition, nanowire, gold, polyaniline, porous anodic alumina

ABSTRAKT

Tato diplomová práce je zaměřená na výrobu Au-PANI-Au nanodrátů. Prezentovaná výroba nanodrátů je založená na elektrochemické depozici různých kovů a polymerizaci polyanilínu do porézních šablon z porézní anodické aluminy připravených anodizací hliníku. Teoretická část pojednává o základech elektrochémie a porézní anodické aluminy.

KLÍČOVÁ SLOVA

anodizace, electrochemická depozice, nanodráty, polyanilín, porézní anodická alumina, zlato

LEDNICKÝ, Tomáš *Template assisted electrodeposition of multilayer nanostructures*: master's thesis. Brno: Brno University of Technology, Faculty of Mechanical Engineering, Institute of Physical Engineering, 2014. 81 p. Supervised by Ing. Jan Čechal, Ph.D.

DECLARATION

I declare that I have written my master's thesis on the theme of "Template assisted electrodeposition of multilayer nanostructures" independently, under the guidance of the master's thesis supervisor and using the technical literature and other sources of information which are all quoted in the thesis and detailed in the list of literature at the end of the thesis.

As the author of the master's thesis I furthermore declare that, as regards the creation of this master's thesis, I have not infringed any copyright. In particular, I have not unlawfully encroached on anyone's personal and/or ownership rights and I am fully aware of the consequences in the case of breaking Regulation § 11 and the following of the Copyright Act No 121/2000 Sb., and of the rights related to intellectual property right and changes in some Acts (Intellectual Property Act) and formulated in later regulations, inclusive of the possible consequences resulting from the provisions of Criminal Act No 40/2009 Sb., Section 2, Head VI, Part 4.

Brno ....

(author's signature)

ACKNOWLEDGEMENT

First and foremost I would like to thank my supervisor Dr. Jan Čechal, for his supervising and friendly approach. I also thank the collective of the laboratory of LabSensNano and the Institute of Physical Engineering for creating such a nice working environment. At last but not least, I wish to express my gratitude to my family for their support during my studies.

Brno ....

(author's signature)

CONTENTS

Introduction **13**

1 Electrochemistry **15**
1.1 Ionic Conductors - Electrolytes 15
1.2 Electrochemical Cells 17
1.3 Faraday's Laws 19
1.4 Electrode Reactions 20
1.5 Electrochemical Deposition 22
1.5.1 Deposition of metals 22
1.5.2 Deposition of polyaniline 23
1.5.3 Template assisted electrochemical deposition 25

2 Porous Alumina Templates **27**
2.1 Aluminium Oxides 27
2.2 Porous Alumina 29
2.3 Formation of Porous Anodic Alumina 29
2.4 Chemical Formation of Oxide Film 33
2.5 Structure of Porous Alumina 36
2.6 Applications of Porous Alumina 39

3 Fabrication of Porous Alumina Templates **41**
3.1 Starting Material and its Preparation 42
3.1.1 Preparation of the aluminium sheet 42
3.1.2 Mechanical and chemical polishing 43
3.1.3 Electrochemical polishing 44
3.2 Anodization 45
3.3 Modification of Porous Alumina 49
3.3.1 Preparation of open-through porous alumina 50
3.3.2 Deposition of the working electrode 52
3.4 Fabrication of Gold Nanoparticle Array 54
3.5 Thin Layer Technique 56

4 Electrochemical Depositions **59**
4.1 Experimental setup 59
4.2 Electrochemical Deposition of Materials 60
4.2.1 Electrolytes and materials of deposition 61
4.2.2 Deposition of films 62

4.2.3 Au-PANI-Au nanowires 62
4.2.4 Au-Ni-Au nanowires 66
4.2.5 Chromium and silver deposition 68
4.3 Calculations 69

Conclusion **71**

A Scanning Electron Microscopy **73**

Bibliography **77**

INTRODUCTION

Nanostructured materials, i.e. materials with size in nanometre scale in at least one direction, have attracted a lot of attention worldwide over the past decades as a result of their peculiar and fascinating properties as well as potential applications. There are a large number of opportunities that might be realized by making new types of nanostructures, or simply by down-sizing existing structures into the nano regime. Therefore a giant scientific and commercial effort is currently devoted to the fabrication as well as the analysis of these structures [1].

Nanostructures constitute a bridge between molecules and bulk systems. The main benefit of nanomaterials is miniaturization, which represents the trend in a broad range of technologies and leads to lower consumption of materials and space. Furthermore, the physical and chemical properties of nanomaterials can differ significantly from those of bulk materials of the same composition. It is generally accepted that quantum confinement of electrons within nanostructures may provide one of the most powerful (and yet versatile) means to control the electrical, optical, magnetic, and thermoelectric properties of the nanostructured materials.

One of the best known and most widespread classes of nanomaterial structures are planar structures (2D), which are an inherent part of the surface finishing industry, the semiconductor industry, etc. On the other hand, the nanowires (1D) and the nanodots (0D) did not attract much of commercial interest. The main issues nowadays are the economical challenges of research and fabrication together with an absence of numerous studies detailing general properties, health impact, biological compatibility. Therefore, with the increasing demand for nanowires a considerable study of a fabrication methods is required.

The general aim of this work is to present a very versatile, economically friendly and relatively simple method for the fabrication of nanowires. Using this method, it is possible to fabricate an array of uniform nanowires for which the chemical composition, structure, and morphology can by adjusted to fulfil specified requirements.

The primary goal of this work is to fabricate multi-segment nanowires consisting of two conducting parts (antennas) with a thin non-conducting gap (example illustrated in Figure 1). This system was inspired by Sheldon and Atwater theoretical work on plasmoelectric effect [2], the study of split-dipole gold nanoantennas with polymer gap by O'Carroll [3], and works on Au–NiO–Au segments nanowires by Tresback [4] and Perego [5]. It is believed that predicted electro-optical properties can lead to possible applications in sensors or solar cells.

In this work we have chosen fabrication of nanowires based on electrochemical deposition within the porous anodic alumina templates. Therefore, in chapter 1 we go through basics of the electrochemistry. Afterwards, in chapter 2 we focus on the

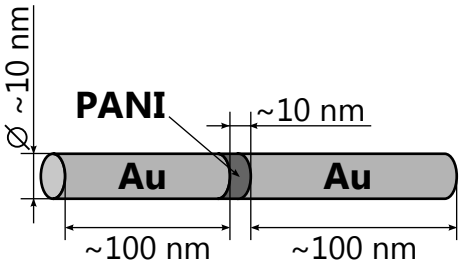

Fig. 1: Schematic view of the multi-segment nanowire composed of two gold (Au) segments separated by polyaniline (PANI) part.

formation process and description of the porous anodic alumina (PAA). The practical part begins with chapter 3 where we describe the fabrication process of the porous anodic alumina templates and discuss the benefits of the individual methods and the achieved results. At the end, in chapter 4 we discuss the electrochemical deposition of various materials within the porous templates which leads into formation of the array of nanowires.

1 ELECTROCHEMISTRY

Electrochemistry is a branch of chemistry concerned with the interrelations between electrical and chemical effects. The theory presented in this chapter is thoroughly explained in the books: Fundamental of Electrochemistry [6] and Electrochemical Methods [7]. The main topic of electrochemistry is the investigation of properties of ionic conductors and their electric circuits, and the investigation of phenomena occurring during passing of electric current through these circuits. The ionic conductors in the liquid phase are also known as electrolytes. In contrast to the electronic conductors (metals, carbon materials, etc.) where the charge carriers are electrons (and holes), the ionic conductors consist additionally of mobile ions (atoms or molecules with a positive or negative charge). The most widely used and most thoroughly studied ionic conductors are aqueous solutions of acids, bases, and salts.

The ability to control charge carriers, especially the ions of electrolytes, by the electric field with the combination of electrochemical reactions occurring on the interface between electrolyte and electric conductor, results in powerful methods of the electronic conductor surface modification.

In this work, these methods were used to fabricate the porous template as well as the nanowires. Therefore, in this chapter, we focus on the fundamental theory of electrochemistry required and used in the practical part of this work.

1.1 Ionic Conductors - Electrolytes

The aqueous electrolytes are solutions of acids, bases, and salt ions dissociated in water. This dissociation can be either complete or partial. To describe this process we can write the simple dissociation equation:

$$\mathrm{M}_{\tau_+}\mathrm{A}_{\tau_-} \rightleftharpoons \tau_+\mathrm{M}^{z_+} + \tau_-\mathrm{A}^{z_-}, \tag{1.1}$$

where M^{z_+} is the cation of the dissociated acids (H^+), bases (K^+, Na^+, Ca^{2+}) or salts (e.g. cations of metals: Cu^{2+}, Fe^{3+}, Au^+, Ni^+), and A^{z_-} is the anion of the acids (SO_4^{2-}, HPO_4^{2-}, $(\mathrm{COO})_2^{2-}$), bases (OH^-), and salts (ClO_4^-, $(\mathrm{CN})^{2-}$). It is evident that $z_+\tau_+ = z_-\tau_- = z_\tau$, where z_τ is the electrolyte's charge number.

Like all equilibria, the electrolyte's ion dissociation reaction has a particular equilibrium constant, called the dissociation constant (K), which is defined as the ratio of the concentration between reactants to the products of the reaction:

$$K = \frac{[M^{z_+}][A^{z_-}]}{[M_{\tau_+}A_{\tau_-}]}. \tag{1.2}$$

From the definition it is clear, that as the dissociation constant approaches zero, the reaction is inhibited, thus the concentration of the reactant is 100 % (complete

dissociation). On the other side, when the dissociation constant approaches infinity, the reaction tends to form 100 % products. This equilibrium, according to electrolyte composition, can be easily shifted by temperature causing increase or decrease of the charge carriers. This relationship is closely tied to the electric properties of the electrolyte.

Electric current in an electrolyte is the directed motion of the ions under the influence of an applied electric field. Without the applied electric field the motion of the ions is chaotic (thermal, diffusion, etc.). When an electrostatic field ($\vec{E}$) is applied, each charge (q) carrier finds itself under the effect of an electric driving force

$$\vec{F} = q\vec{E}, \tag{1.3}$$

causing the ions to move in the direction given by the field. This collective movement of charge carries represents the electric current within the electrolyte.

An important parameter for the electrolyte is its conductivity. A convenient parameter for its characterization is the current density (J) that is independent of conductor dimensions. It is commonly accepted to define it as:

$$J \equiv \frac{I}{S_{\mathrm{WE}}}, \tag{1.4}$$

where I is total current on the surface area of the working electrode S_{WE}. The working electrode (detailed in the next section) is the electric conductor in contact with the electrolyte. The current density J is one of the fundamental parameters in electrochemistry. The SI units of the current density are Am^{-2}, but more convenient units are mAcm^{-2}. The current density is proportional to the electric field strength:

$$\vec{J} = \sigma\vec{E}. \tag{1.5}$$

The factor of proportionality σ is the (electrical) conductivity (units: Scm^{-1}). Because the conductivity is closely related to the mobility of the charge carriers (ions, electrons) it depends on the temperature of the electrolyte. Moreover, as expected with the rising concentration of the ions, the conductivity also increases and vice versa. This fact is fundamental for the further understanding of electrochemical processes, where the ions of the electrolyte are consumed, thus the concentration is changing with time. For this purpose it is required to describe the system (the electrochemical cell) where these processes occur.

1.2 Electrochemical Cells

An electrical circuit including at least one ionic conductor is called an electrochemical cell (galvanic cell or electrolytic cell). However, the term galvanic cell is traditionally used for cells where the chemical energy is converted into the electrical energy (battery, fuel cell). By contrast, the cell where the electric energy is convert into chemical energy is called an electrolytic cell. The scheme of both types is illustrated in Figure 1.1. In the galvanic cell the redox reaction is spontaneous and it is responsible for the production of electrical energy. However, in the electrolysis cell the redox reaction is initiated and driven by electrical energy.

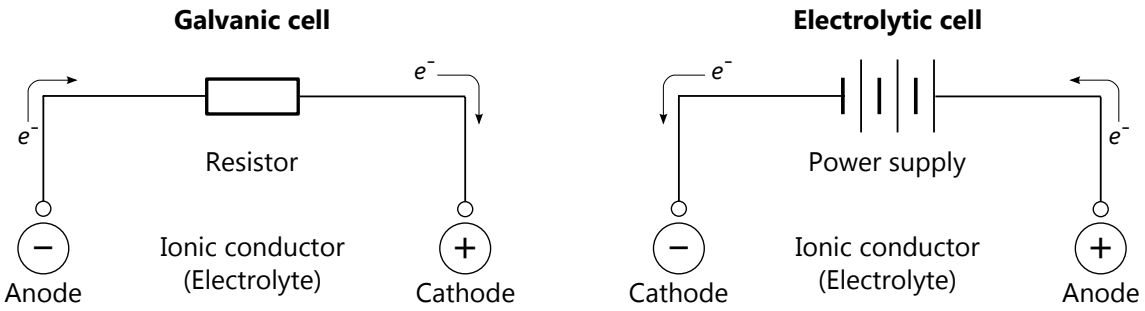

Fig. 1.1: Scheme of the galvanic and electrolytic cells. (Adopted according to [7].)

In this work we will focus only on the electrolytic cell (illustrated in Figure 1.2 in more detail), which is employed for the fabrication of the templates and nanowires. The electrolytic cell consists of two electric conductors (electrodes) connected to the source of electric current (power supply), which are in direct contact with the ionic conductor (electrolyte). It is expected, from the nature of electric force ($\vec{F} = q\vec{E}$), that the positive charge carriers (cations) are attracted to the negative electrode. At the moment when they reach the electrolyte/electrode interface they accept electrons from the negatively charged electrode. This current flow from the electrolyte to the electrode is simultaneously (in the ideal case) compensated by the corresponding charge transfer carried by anions (and electrons) on the positive electrode. An electrode from which the current flows to the electrolyte is called anode (from Greek $\alpha\nu\alpha$, "up"), while an electrode to which the current from electrolyte flows is called cathode (from Greek $\kappa\alpha\tau\alpha$, "down").

The electrolytic cells are frequently employed to carry out desired chemical reactions at the expense of electrical energy. This energy is controlled by the current passing through the electrolyte (galvanostatic mode) or the potential of the electrodes (potentiostatic mode). The electrode, where the reactions of interest occur, is called working electrode the (WE). The other electrode is called the counter electrode (CE), which in the two-electrode cell (example shown in Figures 1.2 and 1.3)

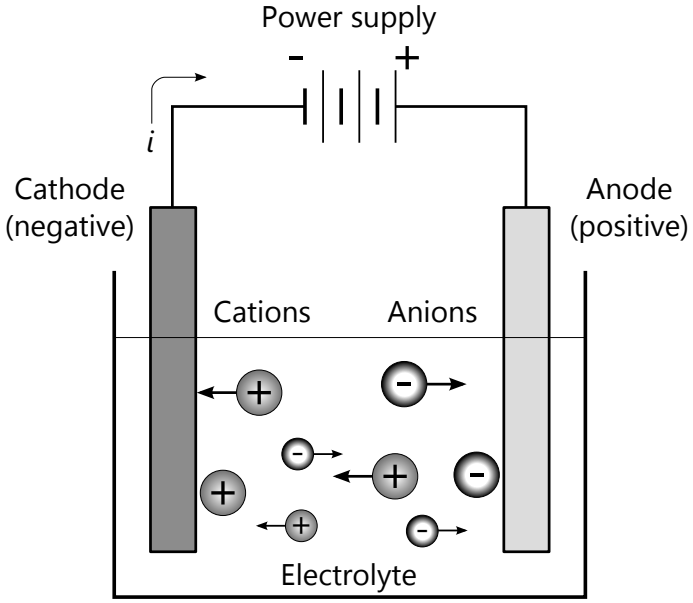

Fig. 1.2: Schematic illustration of the electrolytic cell.

functions as both the reference (RE) and auxiliary electrode (AE). This simple setup is sufficient in most applications even though it has one major drawback - the known (measured) potential differs from the real potential of the CE. The main cause of this behaviour are redox reactions on the electrolyte/electrode (CE) interface which are accompanied by the current flow. This is a fundamental problem of potential measurement. In addition, polarization of the electrolyte molecules can occur at the interface, which adds an additional error into the measurement. Thus, it is unsuitable for precise potentiostatic experiments, systems featuring the electrolytes with high electrical resistance (nonaqueous solution) or electrolytic cells where the AE's surface is comparable or smaller than the WE's surface.

To solve this problem, the roles of supplying electrons and providing a reference potential are divided between two separate electrodes. The RE's role is to act as reference in measuring and controlling the WE potential but no current passes through it. Instead, all the current passes through the AE. Those electrodes (WE, AE, RE) make up the three-electrode cell (illustrated in the Figure 1.3). The RE is a half cell with a known reduction potential. The saturated calomel electrode (SCE) and copper-copper(II) sulfate electrode (CSE) are frequently used for this purpose. To minimize the ohmic potential drop, it is important to place the RE close to the WE. This change of the potential, together with the complex character of the RE, contributes to more complicated practical solutions.

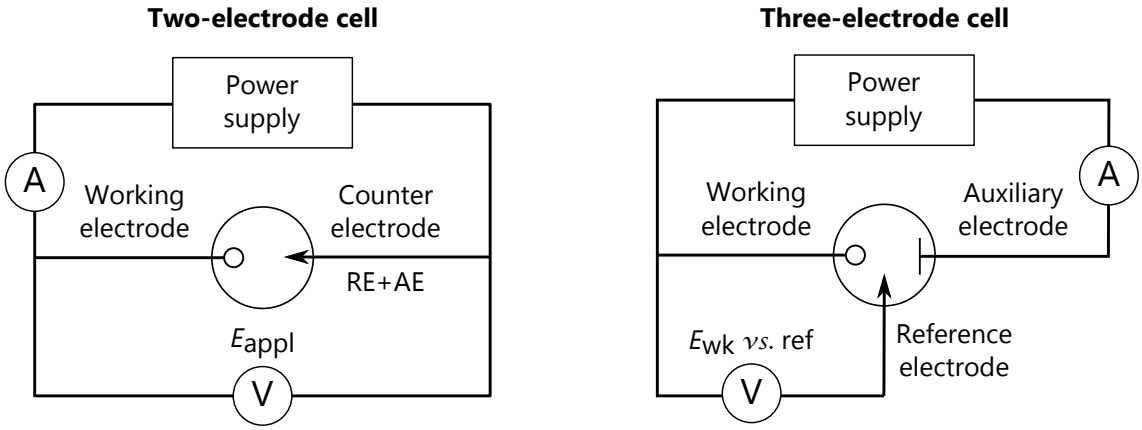

Fig. 1.3: Schematic view of the two-electrode cell versus three-electrode cell. In the two-electrode cell all current flows through the WE and CE while the applied voltage is measured between them. In the three-electrode cell the voltage is measured between RE and WE while the current passes through the AE and WE. (According to [7].)

1.3 Faraday's Laws

In the electrolytic cell, two types of processes occur - the faradaic and the nonfaradaic process. To distinguish between them it is necessary to interpret Faraday's laws, which were formulated by Michael Faraday in 1832–1833 [9].

Faraday's first law reads: In electrolysis, the quantities of substances involved in the chemical change are proportional to the quantity of the electricity which passes through the electrolyte.

Faraday's second law reads: The masses of different substances set free or dissolved by a given amount of electricity are proportional to their chemical equivalents.

The conclusion from the Faraday's laws is that the mass of reactant involved in an electrode reaction is related stoichiometrically to the number of charges (electrons) transferred through the circuit. This result can be formulated as the equation

$$m = \frac{QM}{z\mathrm{F}}, \tag{1.6}$$

where m is mass of the formed or reacted substance, Q is the charge consumed by the reaction ($I = \mathrm{d}Q/\mathrm{d}t$, where I is the electric current and t is time), z is the charge number of the ion and F is the Faraday constant ($\mathrm{F} = \mathrm{N_A e} \approx 9.65 \cdot 10^4\,\mathrm{Cmol^{-1}}$) [8].

Faraday's laws are absolutely rigorous for steady currents. They are the basis for a highly accurate method of measuring the amount of charge (coulometry). However, a deviation from Faraday's laws caused by transient currents can be observed in electrolytic cells (see the next section). To include the deviation into the calculation without significant changes, the efficiency η of the reaction is introduced. The

reaction's efficiency specifies the ratio between the real and the theoretical (according to (1.6)) amount of the reaction's product [9].

1.4 Electrode Reactions

Since the electrolytic cell and the reactions within form a complex system, it is convenient to focus on only one-half of the cell at a time. As a result we can simplify the problem only to the reactions on one electrode. If necessary, the behaviour of a whole cell can be obtained by combining the characteristics of the individual half-cells.[7]

The electrode reaction that will occur depends on both the electrode and the electrolyte, and also on external conditions (applied current or voltage, temperature, pressure, etc.). These reactions are divided into two categories by the character of the process. The first kind is characterized by charge transfer across the electrode/electrolyte interface. Electron transfer causes oxidation and reduction to occur. Since such reactions are governed by Faraday's law, they are called faradaic processes. Other processes such as adsorption or desorption can occur, and the structure of the electrolyte/electrode interface can change with the charging potential or electrolyte composition without charge crossing through the electrode's interface. These processes are called nonfaradaic processes. However, the term parasitic reaction is frequently used to emphasize the primary interest on the faradaic reactions. Also, in this work we will focus only on the faradaic reactions (oxidation and reduction).

These electrochemical reactions are heterogenous, hence they do not occur throughout the entire volume of the electrolyte, but only near the electrolyte/electrode interface. Thanks to this effect, the electrochemical deposition of metals (electroplating) and oxidation are one of the key methods of surface finishing. This interface can be simply described by chemical notation, e.g. (H_2SO_4,aq|Al), ($NiSO_4$,aq|Me). The electrolyte is usually characterized by the component of interest which is set before the vertical bar. For example $NiSO_4$,aq| represents Watts bath which is a solution of $NiSO_4$, $NiCl_2$, and H_3BO_3. However, in the reaction the main reactant on the metal electrode (noted after vertical bar) is Ni^{2+} which is predominantly donated by $NiSO_4$. The solvents (H_2O) and buffers (H_3BO_3) are frequently omitted in the interpretation of electrochemical reactions and processes.

The oxidation occurs at the anode. The example (1.7) illustrates oxidation of the aluminium (Al) anode in the aqueous solution of sulfuric acid (H_2SO_4). This widespread industrial method for passivation of aluminium alloys is called anodiza-

tion. The anodization will be discussed in the chapter 2 in detail.

$$\text{Anode } (\mathrm{H_2SO_4}, aq|\mathrm{Al}): \quad 2\,\mathrm{Al} + 3\,\mathrm{O^{2-}} \longrightarrow \mathrm{Al_2O_3} + 6\,\mathrm{e^-} \tag{1.7}$$

The aluminium is not the only metal that form oxides in such conditions. On the contrary, almost every metal (Cu, Zn, Ni, Fe, etc.), and especially the valve metals (Ti, W, Ta, Nb, etc.), can be oxidized this way. This behaviour in the combination of other unique properties are nowadays widely studied in order to fabricate nanomaterials, e.g. $\mathrm{WO_3}$ nanodots [10], and $\mathrm{TiO_2}$ nanorods [11].

The less common products of the oxidation are gases evolved from anions or the anode material. Therefore, it is important to evaluate the safety risk, especially in case of chloride ($2\,\mathrm{Cl^-} \longrightarrow \mathrm{Cl_2} + 2\,\mathrm{e^-}$), and any other toxic or dangerous fumes.

On the other hand, the reduction takes place at the cathode. The most significant process of interest is electrochemical deposition. During the deposition, the metal cations ($\mathrm{Me^{z+}}$) of the electrolyte migrate toward the cathode, where they are reduced to zero valence state. This can be expressed as

$$\text{Cathode:} \qquad \mathrm{Me^{z+}(aq)} + \mathrm{ze^-} \longrightarrow \mathrm{Me(s)}. \tag{1.8}$$

The example (1.9) describes the electrochemical deposition of the nickel (Ni) from the solution (Watts bath). The final structure and composition of the deposited layer depends on many factors. The crucial ones are the cathode surface, the electrolyte composition and conditions of the deposition (current density, temperature, etc.).

$$\text{Cathode } (\mathrm{NiSO_4}, aq|\mathrm{Me}): \qquad \mathrm{Ni^{2+}} + 2\,\mathrm{e^-} \longrightarrow \mathrm{Ni} \tag{1.9}$$

It is important to emphasize that the electrode can be the reactant as well as the product of the reaction. This situation is illustrated on the gold electroplating cell, where in this case the electrolyte is the aqueous solution of gold potassium cyanide ($\mathrm{KAu(CN)_2}$) [12]. For the purpose of this illustration, it is not required to understand the complexity of the electrode reactions, therefore it will be discussed later (in the section 1.5.1).

$$\text{Cathode } (\mathrm{KAu(CN)_2}, aq|\mathrm{Au}): \quad \mathrm{[Au(CN)_2]^-} + \mathrm{e^-} \longrightarrow \mathrm{Au} + 2\,\mathrm{CN^-} \tag{1.10a}$$

$$\text{Anode } (\mathrm{KAu(CN)_2}, aq|\mathrm{Au}): \quad \mathrm{Au} + 2\,\mathrm{CN^-} \longrightarrow \mathrm{[Au(CN)_2]^-} + \mathrm{e^-} \tag{1.10b}$$

On the electrolyte/cathode interface (1.10a), the gold from the complex is reduced at the cathode ($\mathrm{Au^+} \longrightarrow \mathrm{Au^0}$). The deposited material (Au) is same as the cathode material, thus the electrode is product of the reaction. On the other side, at the electrolyte/anode interface (1.10b), the electrode material (Au) is chemically involved in the electrode reaction. Such electrodes are called consumable electrodes (which is the same as the aluminium anode in the example 1.7).

A similar example is described by equation (1.11a) and (1.11b). However, now the electrode material (Pt) is not chemically involved in the reaction, but it is still a source of electrons. Such electrodes are called nonconsumable.

$$\text{Cathode } (KAu(CN)_2, aq|Pt): \quad 4\,[Au(CN)_2]^- + 4\,e^- \longrightarrow 4\,Au + 8\,CN^- \tag{1.11a}$$

$$\text{Anode } (KAu(CN)_2, aq|Pt): \quad 2\,H_2O \longrightarrow 4\,H^+ + O_2 + e^- \tag{1.11b}$$

The choice of the electrode material depends on the electrolyte and the application. The consumable electrodes help to maintain the composition of the electrolyte. This is especially important in the applications where the amount of the deposited material is crucial parameter and the electrolyte is not frequently changed, which is why the continuous regeneration is required. The nonconsumable electrodes are highly preferable in the scientific research and the fields where the high purity of a deposited material is desired. In industry, carbon and lead electrodes are widely used mainly because of their low costs. However, more suitable for the experimental research are the stainless steel, silver, gold or platinum electrodes.

1.5 Electrochemical Deposition

The main methods of fabrication used in this work are the anodization of aluminium and deposition of various materials (gold, nickel, polyaniline, etc.). Thus, in this section, we will briefly focus on the deposition processes while the anodization will be described in chapter 2. The deposition is characterized by reduction or oxidation reactions which are accompanied by phase transition from the electrolyte (liquid) phase to the solid phase, or a polymerization in case of monomers.

1.5.1 Deposition of metals

The basic principles of the ion migration and reduction reactions were described in previous section. However, this simple electrode/electrolyte interface cannot fully explain the deposition of metals on a cathode which form very stable coordinate complexes in the electrolytes ($[Au(CN)_2]^-$).

The process, describing the attraction of the negative ion complex to the cathode and its breakup, is illustrated in Figure 1.4. The Helmholtz double layer, which is formed by the absorbed cations at the cathode surface, plays the main role in this process. For the characterization of this double layer a few models were proposed which are described in [6, 7, 13] in detail. The negatively charged complex ions (e.g. $[Au(CN)_2]^-$ present in the gold plating baths) approaching this layer become polarized in the electric field of the cathode (Figure 1.4c). Finally, within the Helmholtz layer the complex breaks up (Figure 1.4d). Its component, ligand ions or molecules,

are freed while the metal is released in the form of a positively charged cation which is deposited as the metal atom on the cathode (Figure 1.4e) [14].

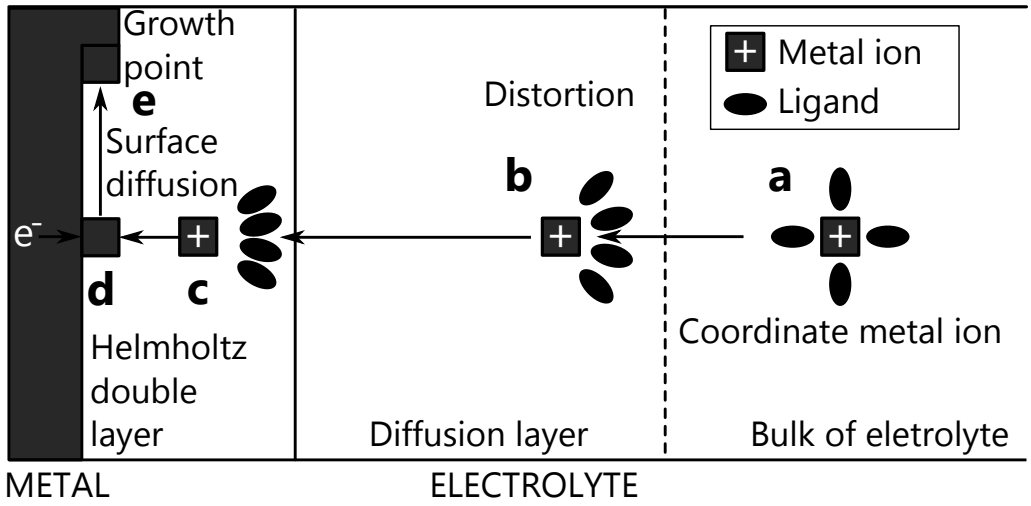

Fig. 1.4: Schematic diagram of deposition process: the metal ion in its ligand field (a), the ligand field becomes distorted (b), the metal ion is stripped from its ligand field (c), the neutralization of the metal ion (d), the metal atom migrates to the nearest growth point (e). (According to [14].)

Although this example was illustrated on the gold(I) cyanide complex, in principle it also describes the deposition of other materials forming various complexes in electrolyte. It is expected that the easiness (potential of electrodes, temperature, etc.) of the deposition of specific material will depend on the fact how easy these ions dissociate from the complex.

1.5.2 Deposition of polyaniline

A diametrically opposite type of deposition is oxidative polymerization of aniline which results in formation of polyaniline (PANI). The primary reaction is oxidation of aniline monomer (shown in Figure 1.5) forming dimeric species which leads to the formation of a oligomers and polymer. Compared to the electrochemical deposition of metals the polymerization can occur throughout the entire electrolyte. This is caused by migration of radical, however the probability decreases rapidly from the electrode surface, where the monomers and oligomers are oxidized, due to the high radical reactivity.

Polyaniline can occur in one of three idealized oxidation states: leucoemeraldine (colorless), emeraldine(green/blue), and (per)nigraniline (blue/violet). Additionally, the last two states can occur in a salt or a base form (emeraldine example is shown in Figure 1.6). The salt can be deprotonated in alkaline to its base which can be again

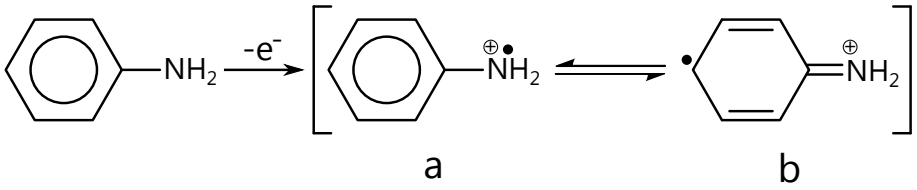

Fig. 1.5: The oxidation of the aniline monomers resulting in radicals (a,b) – initiation. The recombination of the radicals (a,b) form dimeric species which subsequent oxidation and recombination leads to polymer growth – propagation. The mechanism is fully described in [15].

reprotonated with acids (HA) to corresponding salts. These states of PANI differ significantly in the color as well as their electrical conductivity. The easy transition between the conducting emeraldine salt (ES) and its non-conductive emeraldine base (EB) was a primary reason for PANI choice as the separating segment between the gold parts (plasmonic antennas) in this work.

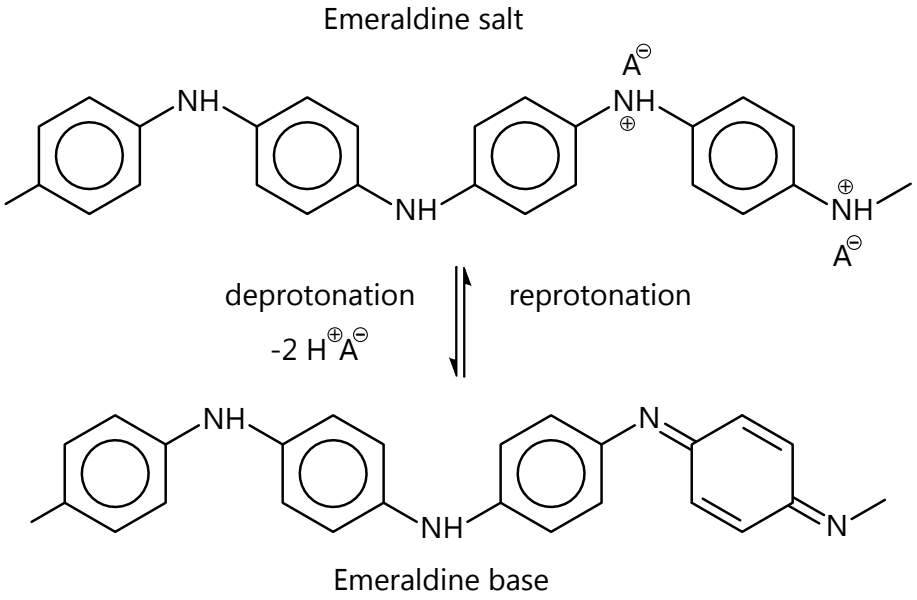

Fig. 1.6: Two of the polyaniline (PANI) forms: the doped (protonated) green and conducting form is called emeraldine salt (ES); and the neutral, blue and non-conducting form is called emeraldine base (EB). (According to [16].)

The polymerization of aniline is usually done in acidic electrolytes. This ensures a good solubility of aniline and a high conductivity of the electrolyte, but more importantly the acidic solution protonates the formed PANI, thus increases its electrical conductivity. In constrast to proposed electrochemical deposition of metals, the polymerization takes place on the anode (oxidation). This fact is in general

very restrictive in respect to the material of WE. In combination with an acidic electrolyte, this excludes all materials which are easily oxidized (Al, Cu, Ni, Fe, etc.). This will be discussed in the result section of chapter 4.

1.5.3 Template assisted electrochemical deposition

At the end of this chapter, we will briefly discuss the electrochemical deposition from the application point of view. This process usually leads to the formation of a macroscopically compact layer on the WE, which is illustrated in Figure 1.7(left). In the examples shown in Figure 1.7 the electrolyte/electrode interface is represented only by the top side of WE.

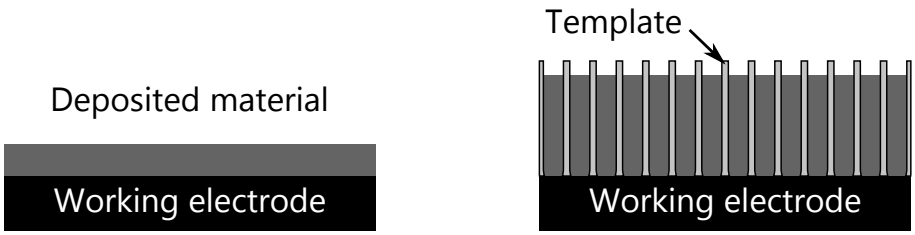

Fig. 1.7: Illustration of the electrochemical deposition of layer (left) and structures predefined by the template (right).

The template assisted electrochemical deposition can be characterized as simultaneous depositions on an array of working electrodes which are defined by a template. The final structure of the deposited material tends to form a negative mold of the template, and so the porous templates can be used to create arrays of nanowires (Figure 1.7(right)). Moreover, the length of nanowires can by controlled by the deposition conditions, thus it is also possible to obtain the array of nanopillars or nanodots. Unfortunately, from the Faraday's law (1.6) it is expected that wider nanowires will grow slower than thinner one. Therefore, it is important to use the template with a uniform pore diameter to obtain small deviation of the nanowires' length.

For this purpose it is believed that the most suitable are the templates made of porous anodic alumina. The properties and fabrication of these templates will be discussed in the following chapters in more detail.

2 POROUS ALUMINA TEMPLATES

The porous anodic alumina (PAA) as a product of the anodization (anodic oxidation) of aluminium is nowadays one of the most widely recognized and used templates for the fabrication of nanowires (nanodots, nanopillars, etc.) by the electrochemical deposition (or oxidation). In this chapter we go through the brief origin, formation, structure, and applications of this layer. This chapter is based on the complex work of G. D. Sulka [17] and is extended by experimental observations and results.

2.1 Aluminium Oxides

Aluminium (Al) and its alloys have, since the end of 19th century, attracted considerable attention because of their good mechanical properties and relatively easy fabrication. Because of the high affinity of the aluminium surface to oxygen, the metal is always covered with a very thin, compact and highly resistant oxide film. The thickness of this native oxide layer is usually 2–4 nm. In the past century a lot of efforts have been made to study and modify this layer and to change its mechanical properties, chemical resistance, color, adhesion, etc.

One of the most common methods is electrochemical oxidation, called anodization. This technique has been used commercially for the preparation of protective or decorative layers on the aluminium surfaces since 1923 [18]. The resulting structure and composition of the anodic aluminium oxide (AAO) depends on the electrolyte, electric field, temperature, anodization time and other conditions.

Two basic types of anodic oxides can be prepared: dense and compact barrier-type film or porous-type film (illustrated in the Figure 2.1). These two types of films differ in structure and the limiting thickness that can be produced. Apart from the temperature of the electrolyte, the thickness of barrier-type film is controlled solely

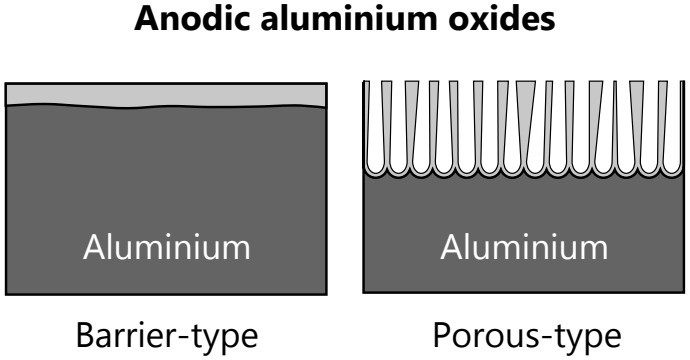

Fig. 2.1: Schematic representation of barrier-type and porous-type anodic aluminium oxide morphology.

by the applied voltage, whereas the thickness of porous-type film depends mainly upon the current density and time of the anodization. The maximum achievable film thickness for barrier-type films is restricted by oxide breakdown voltage (500–700 V), thus the limiting thickness corresponds to 700–1000 nm [19]. The thickness of porous films, being time dependent, is theoretically unlimited.

Moreover the nature of the electrolytes which produce these films differ significantly. Electrolytes in which the formed oxide film is completely insoluble are electrolytes which produce barrier-type films; examples include neutral boric acid (H_3BO_3) solution, ammonium borate ($(NH_4)_2B_4O_7$), and several organic electrolytes including citric ($C_6H_8O_7$), malic ($C_4H_6O_5$) or glycolic ($C_2H_4O_3$) acids. The neutrality (pH 5–7) is important, especially in the case of organic acids, because it is thought that in strongly acidic solutions these electrolytes do not form completely nonporous barrier-type films. This is tied closely with the nature of the electrolytes which form porous-type films. In these electrolytes, the anodic oxide is slightly soluble. The most commercially important are sulfuric (H_2SO_4), phosphoric (H_3PO_4), chromic ($CrO_3 + H_2SO_4 + H_2O$), and oxalic ($C_2H_2O_4$) acids at almost any concentration [19].

Generally, for most anodizing electrolytes, relationships between current density and bulk electrolyte pH exist, delineating porous-type or barrier-type films growth (shown in the Figure 2.2) [20].

In this work we focus on porous-type AAO, called porous alumina. In recent years, porous alumina has attracted considerable research not only because of its importance in the surface finishing of aluminium, but also because of its microstructure.

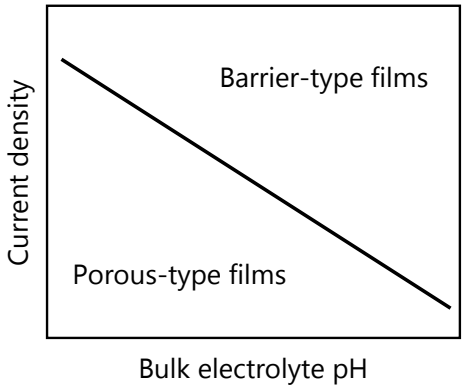

Fig. 2.2: Schematic diagram showing the relationship between solution pH and current density for barrier-type and porous-type anodic alumina formation. The current densities are typically in the $mAcm^{-2}$ range over pH range between 0–7. (According to [20].)

2.2 Porous Alumina

Porous anodic alumina films were first reported by Keller et al [21], who described the formation of nanopore arrays grown perpendicularly to the aluminium surface with relatively low regularity. Since then it took almost 50 years to prepare an almost ideal PAA (shown in the Figure 2.10), which was demonstrated by Masuda and Fukuda [22] by long-time anodization of hight purity (99.99%) aluminium. The two-step anodization process, which has ropidly grown in popularity was presented one year later, in 1996, by Masuda and Satoh [23]. Nowadays, two-step anodization is the most common method to prepare highly and hexagonally ordered nanopore arrays with straight and uniform pores throughout whole PAA thickness.

2.3 Formation of Porous Anodic Alumina

In this section we will discuss the macroscopic formation of PAA. The porous anodic alumina is formed by anodizing aluminium at a constant current density (galvanostatic) or a constant potential (potentiostatic). However, in practice the galvanostatic anodization is not widely used because it is easier to control the reaction (and pore diameter) by the anodizing potential rather than calculating the current for different sample areas. A typical dependence of potential and current density on time during potentiostatic and galvanostatic regime is shown in Figure 2.3A and Figure 2.3B, respectively.

When the constant potential is applied during the initial stage (Figure 2.3, stage a), the current density decreases linearly with time. This linear decrease is associated with a linear growth of high-resistivity barrier-type oxide film thickness on the aluminium surface. Further anodization (stage b) results in the propagation of individual paths (pore precursors) through the barrier film. This process is caused mainly by dissolution of oxide in acidic electrolyte enhanced by the electric field. At the minimum of current density (stage c) the breakdown of the barrier film occurs and the porous structure begins to form. This process is clearly illustrated in the galvanostatic regime (Figure 2.3A), when the potential reaches the maximum – the breakdown voltage of the barrier layer. Subsequently, (in potentiostatic regime) the current density reaches a local maximum due to the rapid oxide formation near the surface. This fast, disordered and unsteady growth of pores is gradually damped in the deeper volume of the aluminium substrate where the steady-state growth occurs (stage d). During this steady stage, the current density and growth rate of pores are constant. These results (2.3B) are most easily interpreted by two superposed processes (shown in Figure 2.4); the first exponential decrease is connected with barrier film formation, and the second represents the process of pore formation.

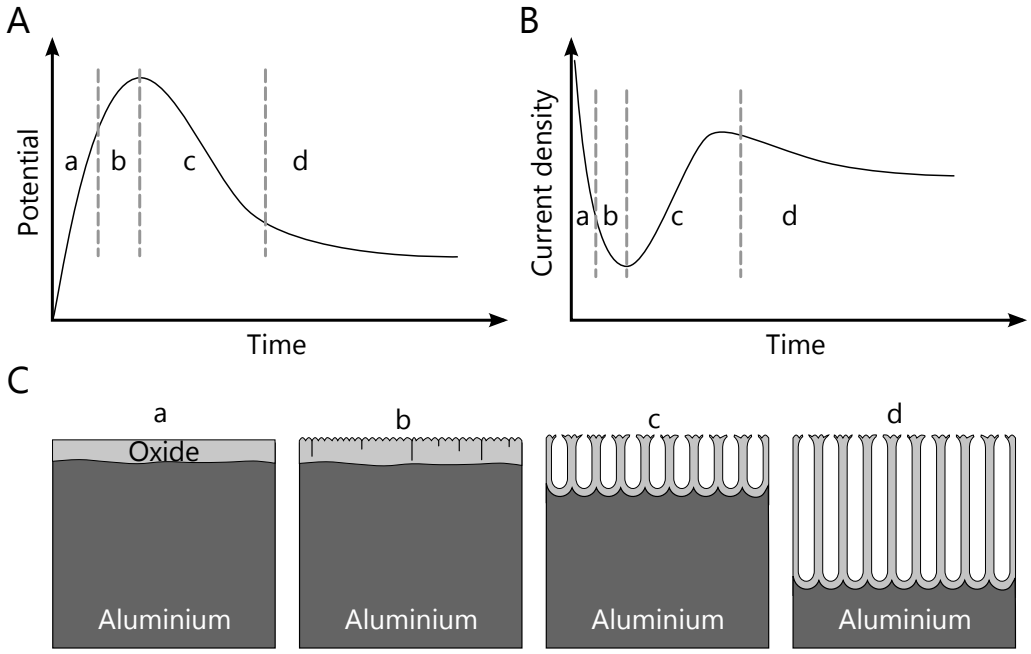

Fig. 2.3: Schematic diagrams and illustration of kinetics of PAA growth in galvanostatic (A), potentiostatic (B) regimes, and stages of PAA development (C). (According to [17].)

Although the anodization of aluminium was successfully and widely applied for the synthesis of highly-ordered nanostructures, it remains unclear which physical (or chemical) factors control pore ordering during oxide growth and especially pore nucleation. In this work we will not focus on theories proposing various explanations, which are discussed elsewhere [17, 19, 20, 24]. The emphasis will be focused on the macroscopic effects affecting the nucleation of pores and their growth.

It is generally accepted that the initiation of pores starts on the barrier-type oxide (the native layer), thus all effects depend on the structure of this layer. For better illustration and from the practical view these effects will be divided into two categories. The first type of effect result in the nucleation of pores at the place with the lowest electric resistance. This leads to the pore nucleation on the surface defects (grain boundaries, scratches, cracks, pits) and impurities of the material.

Another process (involving migration of ions and distribution of the electric field) increases the probability of nucleation for secondary and tertiary pores at a specific distance from the primary pore. This process is geometrically illustrated in Figure 2.5. The primary pore nucleated solely on the surface defect or impurities (stage a). The secondary pore will preferably nucleate in the distance illustrated by dotted circle around primary pore (stage b). The radius of the circle is approximately twice the barrier thickness [24]. Similarly the tertiary pore nucleation will be most probable on the intersection of those circles (stage c). The additional pores are created

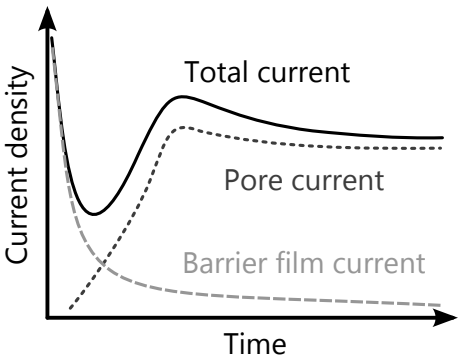

Fig. 2.4: Schematic diagram of overlapping processes occurring during PAA growth in potentiostatic regime. (According to [24].)

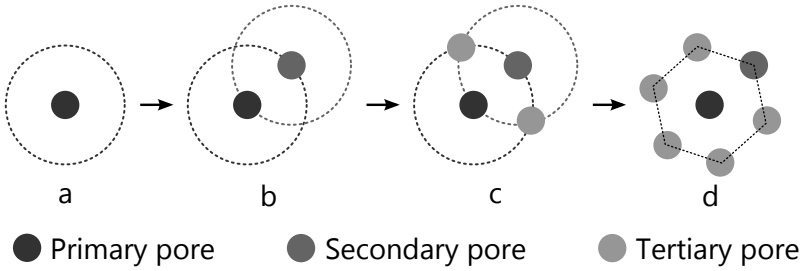

Fig. 2.5: Geometrical illustration of the nucleation of pores on a theoretically perfect aluminium surface.

by the same process, which leads to the hexagonal structure (stage d). From the initial primary pores the nucleation of pores is extended across the whole aluminium surface.

Generally, processes of both types are involved in pore nucleation (on surface defects and enhanced by electric field). Nevertheless, on smooth surfaces like electrochemically polished aluminium or well sputtered aluminium layer the hexagonal structure is predominant (in Figure 2.6(left)). On the other hand, on rough surfaces like mechanically brushed (or polished) aluminium (in Figure 2.6(right)) or pre-treated aluminium surface, the pores nucleate preferably in the scratches or pits. However, the surface pre-treatment cannot fully overcome the hexagonal nucleation. This effect is noticeable in Figure 2.6(right) where nucleation of pores are preferable in the scratches but they are more or less equidistant from each other which leads to the familiar hexagonal pattern.

Before we discuss the growth process, it is necessary to understand the basic effects involved in this process and their consequences. Until the end of this section, we will use the term pore to describe not only the hole in the oxide but also its oxide shell. It is generally accepted that pores grow simultaneously, at the same grow rate and distance from the surface. The major effect behind this behaviour is

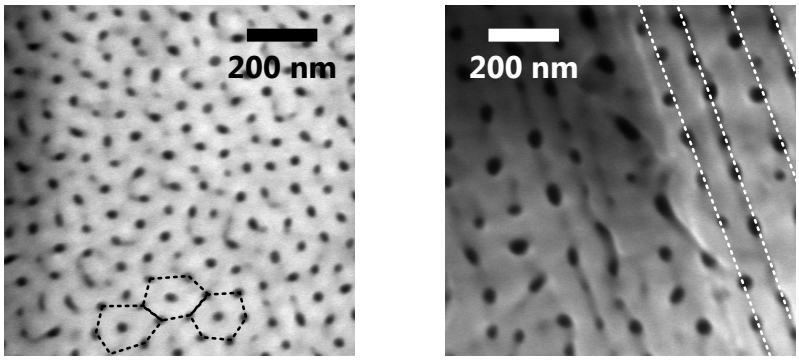

Fig. 2.6: The SEM (Scanning Electron Microscope) images of surface of PAA with illustration of hexagonal (left) and linear (right) pattern (SEM is discussed in the appendix A). Nucleation of pores on the smooth electrochemically polished Al surface(left) and on the rough mechanically brushed Al surface (right). Both anodization were carried out in oxalic acid at potentiostatic regime under 50 V (left) and 70 V (right).

an increasing resistance dependence on the pore's length. This resistance involves several factors like migration of the ions, concentration of electrolyte within pore, etc. As a result, longer pores grow slower than shorter ones.

Another effect is the volume expansion, which is characterized by ratio between volume of growth PAA and volume of consumed aluminium. Because the growth of a pore is restricted by neighborhood pores, this volume expansion is negligible in lateral dimensions and predominant in the height dimension (the thickness). Therefore, it is sometimes referred as the height expansion. However, thanks to this lateral restriction, enormous external forces act on the pores during the growth. On the other hand, the electric field leads to the expansion of pores. As a result the pores growth can be characterized as a competition between those two forces (volume expansion and field assisted oxide formation).

In steady-state growth these forces are in equilibrium while both are relatively stable. Before steady-state is reached, unsteady growth usually takes place. This is expected since the nucleation of pores is primary field assisted while no external force (by volume expansion) is present. This force grows with the depth until it reaches a steady value. This unsteady growth is characterized by disordered growth, while pores change their sizes and positions. The significant mismatch between nucleated and steady-state layout can even lead to branching, merging or termination of nucleated pores (Figure 2.7). The thickness of this disordered layer depends on this mismatch as well as the anodization condition, but usually it is in range of a few micrometers. Consequently, if the pores nucleate from the beginning in the ordered layout (lattice) and anodizing conditions are well chosen the disordered layer will

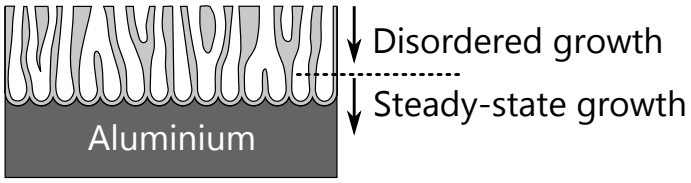

Fig. 2.7: Illustration of disordered layer formed before steady-state growth.

not occur.

The growth of pores usually leads to a hexagonally ordered lattice (honeycomb structure). This structure is the most preferable in respect to the volume expansion. Thus, it is desirable to create nucleation spots (pits) on the aluminium surface in a hexagonal lattice to prevent disordered growth. This is the fundamental idea of the well-known and widespread two-step anodization process (discussed in chapter 3 in detail). However, the hexagonal lattice is not only the possible ordered structure. The square and triangular lattices were prepared by mold imprinting and adjusting the anodizing voltage to match interpore distance with the imprinted lattice parameter [25].

2.4 Chemical Formation of Oxide Film

Anodic oxides (barrier-type and porous-type) formed by the anodization of aluminium are amorphous oxides. The studies showed no presence of crystalline structure of alumina (γ-Al_2O_3 or γ'-Al_2O_3) [17]. Additionally, the anodic alumina is characterized by incorporation of electrolyte ions within its structure, thus it cannot be considered as pure Al_2O_3.

An essential difference between formation of the barrier-type and porous-type oxide is that during the anodization in the acidic electrolyte, not only is there formation of the oxide, but also oxide dissolution occurs. Thus, the pore shell (cell-wall) is formed by the same process as the barrier-type oxide, while the pores are created by guided dissolution of this oxide layer. This leads to the characteristic porous structure of PAA.

Even though the dissolution of the oxide is undesirable for long term anodization and production of narrow pores, it is an important part of the anodization process. Generally, the dissolution can be inhibited by decreasing the temperature. For example anodization in the phosphoric acid can be stopped by decreasing of the temperature to less than approximately 15 °C. On the other hand, enhanced dissolution of oxide, greater than its formation, is required for electrochemical polishing of aluminium (discussed in chapter 3 in detail).

The formation of the aluminium oxide (Al_2O_3) can be written simply as

$$2\,Al + 3\,H_2O \longrightarrow Al_2O_3 + 3\,H_2, \tag{2.1}$$

which represents the overall chemical reaction. Although this reaction is formally correct it does not reflect the details of the whole electrochemical process. A schematic illustration of processes occurring during anodization is shown in Figure 2.8.

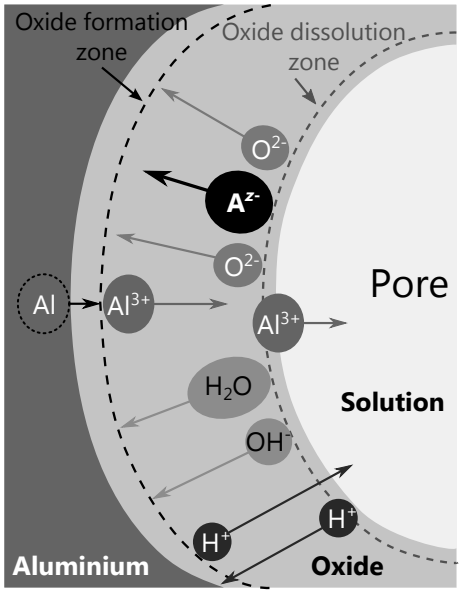

Fig. 2.8: Schematic representation of cross-sectional view and illustration of ions movement through the electrolyte/oxide and oxide/metal interface during the anodization in an acidic electrolyte (in general H_zA). (According to [17].)

It is essential to understand the chemical reactions at the electrolyte/oxide (E/O) and oxide/metal (O/M) interfaces separately. When an electric field is applied, aluminium at the anode's O/M interface is oxidized: $Al \longrightarrow Al^{3+} + 3\,e^-$. On the other hand, the dissociation of water takes place on the cathode: $2\,H_2O + 2\,e^- \longrightarrow 2\,OH^- + H_2$. Moreover, at the E/O interface the creation of OH^- and O^{2-} ions occurs due to H_2O splitting or its interaction with the absorbed electrolyte anions. This can be expressed, in case of sulfuric acid, as: $2\,H_2O + 2\,SO_4^{2-} \longrightarrow O^{2-} + OH^- + H_2SO_4 + HSO_4^-$. Under the electric field OH^- and O^{2-} anions migrate inward through the oxide towards aluminium, where they form an oxide:

$$2\,Al + 6\,OH^- \longrightarrow Al_2O_3 + 3\,H_2O + 6\,e^-, \tag{2.2}$$

$$2\,Al + 3\,O^{2-} \longrightarrow Al_2O_3 + 6\,e^-. \tag{2.3}$$

Although the anodization of aluminium has been investigated widely, it is not clear yet which oxygen-carrying anion species OH^- or O^{2-} ions are involved in the anodic process [17, 26].

Simultaneously with the OH^- and O^{2-} ion migration, outward drift of Al^{3+} cations flux takes part in the oxide formation at the O/M. Depending on the anodizing conditions – and especially on the current efficiency of the oxide growth, which is characterized as a ratio of current consumed for the oxide growth to the total current flowing through the electrolytic cell – oxide formation can also proceed at the E/O interface. For a high current efficiency close to 100 %, and for phosphates and chromate electrolytes, the majority of Al^{3+} are involved in the formation of oxide at the E/O interface. In contrast, for anodizing in oxalate electrolytes accompanied with low current efficiency, the direct ejection of Al^{3+} ions to the electrolyte is preferable. These two processes of the formation of oxide result together with migration of the electrolyte's ions (e.g. SO_4^{2-}, $(COO)_2^{2-}$, PO_4^{3-}, OH^-, H^+) through the oxide layer in two different types of PAA, specifically its cell-wall structure. The most common are duplex and triplex structures of cell-wall (shown in the next section in Figure 2.12). This migration of ions during the formation of the oxide leads to the incorporation (trapping) of these ions within the oxide structure. The typical depth profile of the concentration of different anions is shown in Figure 2.9.

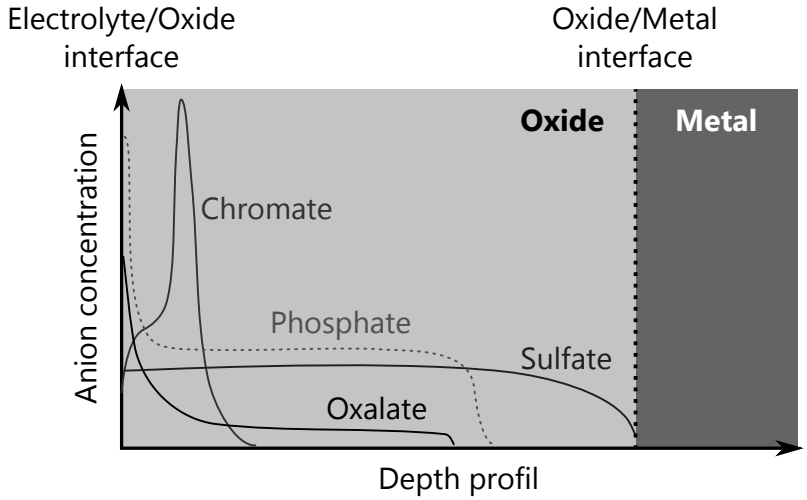

Fig. 2.9: A depth profile of various anion concentrations in the barrier-type oxide film. (According to [17].)

Despite illustrating this case for the barrier-type oxide, it is analogous to the cell-wall structure of pore. This results from the cell-wall forming from the barrier-type oxide. Naturally, these impurities have significant impact on the final properties of PAA (mechanical, optical, chemical). This effect is widely used in industry for coloring of aluminium during its passivation.

2.5 Structure of Porous Alumina

The morphology of ideal porous alumina may be described as a close-packed array of columnar hexagonal cells in a honeycomb arrangement. Each hexagonal cell contains a central pore normal to the substrate, as shown in Figure 2.10. A major benefit is that all dimensions (layer thickness, pore diameter, cell size, barrier layer thickness) can be controlled by anodization conditions or additional methods.

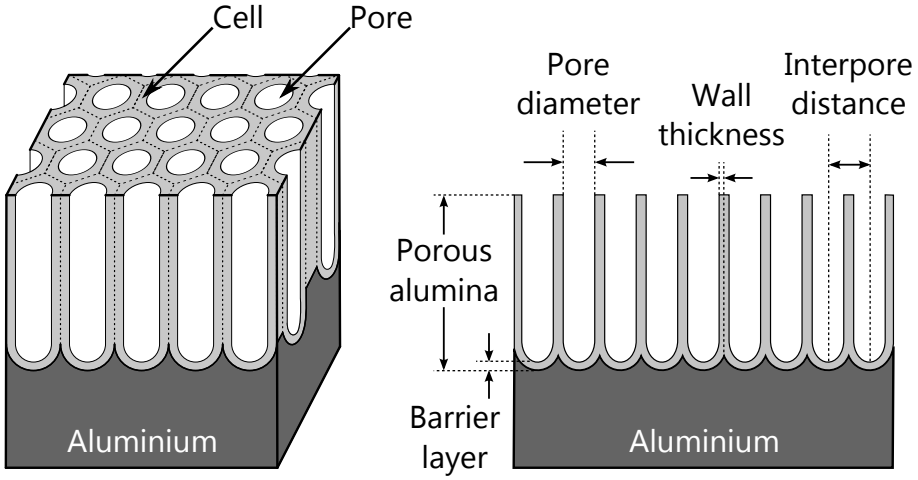

Fig. 2.10: Illustration of the idealized porous alumina on the aluminium substrate. The 3D section view (left) and the cross section view (right). (According to [17].)

One of the most versatile parameters is the pore diameter. Even though the pore diameter mainly depends on the anodization conditions, it can by subsequently widened by chemical etching or narrowed by the atomic layer deposition (ALD). However, cell size depends only on the anodization conditions, thus the pore diameter is always restricted by the cell size (the interpore distance). As a result the uniform pore diameter in range 5–300 nm is achievable. As mentioned, pore diameter depends primarily on the anodization conditions, where the main controlling parameter is the anodization voltage. In a wide range of common temperatures, electrolytes and their concentrations, the pore diameter D_p (units: nm) is linearly proportional to the anodizing potential:

$$D_\mathrm{p} = \lambda_\mathrm{p} \cdot U, \tag{2.4}$$

where λ_p is the proportional constant of approximately 1.1 $\mathrm{nmV^{-1}}$ and U is anodizing potential (units: V). It should be noted that an enhanced chemical dissolution of oxide, resulting in the development of widened pores, occurs during anodizing at a sufficiently high temperature, long anodizing time, or in strong acidic solutions.

The interpore distance D_c (the cell size) is also linearly proportional to the anodization potential:

$$D_c = \lambda_c \cdot U, \tag{2.5}$$

where λ_c is approximately $2.5\,\mathrm{nmV^{-1}}$. This relationship is illustrated by the diagram in Figure 2.11 for various electrolytes. Each electrolyte has a restricted working potential range. This range is limited from above by the break-down voltage of the oxide layer. Above this value the extensive dissolution of oxide leads to an uncontrollable process and the sample burning. On the other hand, the restriction from below is given by value below which the oxidation is radically inhibited. Typical potential range for sulfuric acid is 10–25 V, oxalic acid: 40–80 V, and phosphoric acid: 150–200 V. The extended ranges for these acids in Figure 2.11 illustrated by dotted lines represent so-called hard anodization. During this process the standard voltage is applied at the beginning of the anodization process. After few minutes the potential is rapidly ($\approx\mathrm{Vs^{-1}}$) increased to the final value [17, 27, 28].

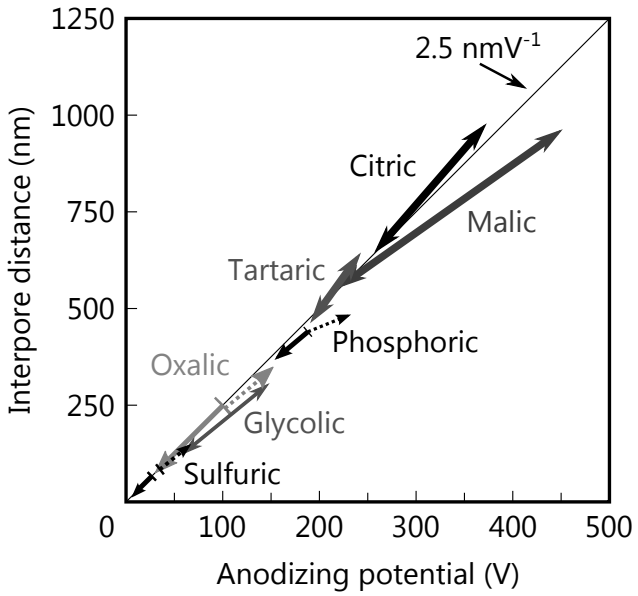

Fig. 2.11: Anodization potential influence on the interpore distance (cell size) for PAA formed in various electrolytes. (According to [17].)

Other morphological features can be simply calculated from pore diameter and interpore distance. For example the cell-wall thickness W is defined as

$$W = \frac{D_c - D_p}{2}. \tag{2.6}$$

As mentioned in previous section, due to ion incorporation within the oxide layer (Figure 2.9), the duplex or triplex structure of cell-walls is formed (shown in Figure 2.12).

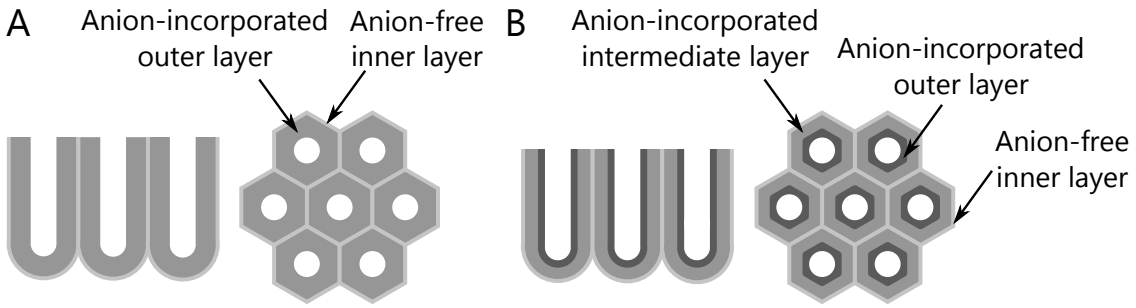

Fig. 2.12: Schematic representations of the sectional and plan view of duplex (A) and triplex (B) structures of porous alumina cell-walls. The duplex structure is typical for anodizing within sulfuric or oxalic acid while triplex structure is formed in phosphoric or chromic acid. (According to [17].)

Another more practical parameter is a porosity α of PAA. It is defined as the ratio of a surface area occupied by pores S_{pores} to the whole surface area S. For ideal PAA with a perfectly circular pore inside each hexagon cell, the porosity can be written as follows:

$$\alpha = \frac{S_{\mathrm{pores}}}{S} = \frac{S_{\mathrm{p}}}{S_{\mathrm{h}}} = \frac{\pi}{2\sqrt{3}} \left(\frac{D_{\mathrm{p}}}{D_{\mathrm{c}}} \right)^2 , \tag{2.7}$$

where S_{p} (units: nm^2) is the area of one pore and S_{h} (units: nm^2) is the area of one hexagon (pore cell). The porosity is an important parameter for electrochemical deposition within PAA because it defines the working electrode surface (discussed in chapter 4 in detail). The porosity of PAA may vary a lot due to various types of pore widening during anodization in different electrolytes or post-treatment procedures (etching of barrier layer). It is usually in the range of 10–40 % or even more in an extreme cases, however the standard values are around 20 %.

An inseparable part of PAA is a very thin, dense and compact barrier layer formed at pore bases. The thickness of this barrier layer B depends on anodizing potential, and is approximately the same as pore diameter:

$$B = \lambda_{\mathrm{b}} \cdot U, \tag{2.8}$$

where proportional constant λ_{b} is approximately $1.0\,\mathrm{nmV}^{-1}$. This compact dielectric layer at the pore bottom makes electrochemical deposition into the pores almost impossible or at least very complicated. On account of this limit, the thickness of the barrier layer is extremely important and can determine further applications or required modifications of PAA.

The last discussed parameter besides an unrestricted surface area, is the thickness of the PAA layer (pore length). In contrast to other dimensions, the thickness of PAA and the anodizing potential are not in a direct relationship. The thickness is

in general coulombically controlled. Thus, it linearly depends on current density, anodizing time and current efficiency. While these attributes depend on electrolyte properties (concentration and composition), temperature, and aluminium substrate, it is practical to determine the final thickness of PAA by experimental measurements. An advantage of this approach is that at the constant anodizing potential (and temperature) the thickness of PAA is always the same for a given anodizing time (and electrolyte) regardless to the anodizing area.

It is important to conclude that a good control of anodizing parameters is essential for reproducible results. This includes especially the stability of the anodizing potential, temperature, and electrolyte composition.

2.6 Applications of Porous Alumina

Thanks to its unique geometrical properties PAA has been in the scientific focus for many years. Porous anodic alumina with a high density of pores is suitable as a template for synthesis of nanostructures, such as: nanowires, nanodots, nanotubes, nanohole arrays, etc. [10, 22, 27]. It can also be modified to create a variety of functional filters [29] or be intergrade into various nanodevices, e.g.: solar cells, photonic crystals or data magnetic storage [17, 30–32].

In this work we describe the fabrication and the modification of porous alumina as the template for electrochemical synthesis of nanowires. The various methods, including preparation of aluminium, anodization process and modification of PAA were studied. The main aim of this work is to present the practical issues, ideas and methods for optimization of PAA fabrication.

3 FABRICATION OF POROUS ALUMINA TEMPLATES

In this chapter we describe the fabrication and modification of porous alumina as the template for the electrochemical deposition of nanowires. The whole procedure is schematically illustrated and briefly described in Figure 3.1. The individual steps will be discussed in individual sections in detail.

Because the fabrication methods (aluminium polishing, anodization conditions, selective etching) and properties of PAA have been well-studied by several researchers, and the results are summarized in many publications (e.g. [17,27,33,34]), the main aim and focus of this work is to present practical issues of PAA fabrication. Various methods were experimentally studied and their results are discussed in respect to the proposed aims. Additionally, while the fabrication is in general a complex procedure, great effort has been put into its optimization.

Most experiments have been done in the laboratory of Microsensors and Nanotechnologies – LabSensNano (Department of Microelectronics, FEEC, BUT). Minor processes have been done in the laboratories and mechanical atelier of the Institute of Physical Engineering (FME, BUT) and in the laboratories of the Institute of Materials Science and Engineering (FME, BUT).

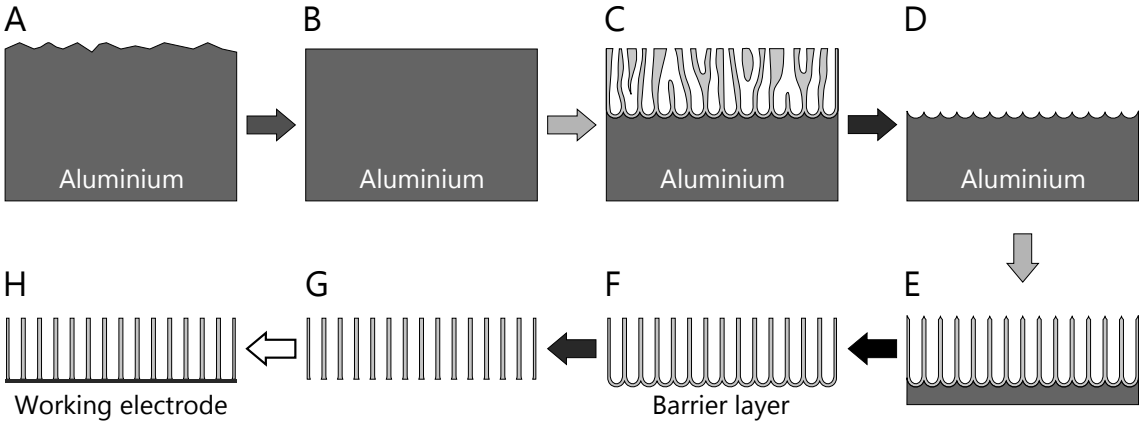

Fig. 3.1: Schematic diagram of fabrication of the PAA template for the electrochemical deposition of nanowires. A starting material (A) is cleaned and polished (B). Then it is anodized (C) and the created PAA is selectively etched. This first step of two-step anodization leads to the pre-patterned aluminium surface (D). The subsequent anodization at the same conditions as first one, creates the well-ordered PAA (E). A removal of the aluminium substrate leads to free standing PAA with the exposed barrier layer (F). The selective removal of the barrier layer is required to achieve an open-through template (G). The last step is deposition of a conducting material as a WE on the bottom side of PAA.

3.1 Starting Material and its Preparation

As a starting material we used high-purity (99.999%), tempered as rolled aluminium sheets ($10\times10\,\mathrm{cm}^2$ and 0.25 mm in thickness) purchased from Goodfellow Cambridge Ltd. The use of aluminium sheets with a purity of 99.95 % resulted in significant decrease of pore order. Moreover, during anodization the impurities from the aluminium precipitate on the top of the PAA surface. Thus, it was decided to use higher purity material to lower the overall contamination. Additionally, sheets with the thicknesses of 0.05 mm, 0.10 mm, and 0.5 mm were tested.

At this point it is necessary to emphasize that the desired thickness of PAA template is approximately 50 µm. This thickness has been decided over time as the thinnest possible for a simple manipulation of PAA.

Thus, the sheets with the thicknesses of 0.05 mm and 0.10 mm are not thick enough for two-step anodization but more importantly, they have a tendency to bend during the fabrication process. On the other hand, the 0.5mm thick sheets are so thick that the time of aluminium etching (Figure 3.1E-F) is extended significantly. In summary, the high-purity aluminium sheets (99.999%) of thickness 0.25 mm were the most suitable from an application as well as an economical perspective.

3.1.1 Preparation of the aluminium sheet

First, the aluminium sheet was cut into specimens with the are of $3.3\times10\,\mathrm{cm}^2$ by a shear (squaring shear) to minimize the bending of aluminium. Our aim was to fabricate as large of an aluminium piece as possible in a single fabrication procedure; the size of the sample was mainly limited by the laboratory equipment (laboratory glass, power supplies).

Because it is more practical to grow a PAA only on one side of an aluminium sheet (Figure 3.1), it is necessary from the beginning to distinguish between the top side (top) and the bottom side (bottom) of the aluminium sheet. The processes applied on top are: surface pre-treatment and the anodization. The bottom is treated by etching processes. This nomenclature is also frequently used for PAA descriptions.

Before any cleaning or polishing of aluminium, it is advantageous to slightly groove (scratch) the top side of specimen by scalpel into mesh of future samples (shown in Figure 3.2). This results in the better controlled cleaving of the final PAA templates in large number of the samples.

Before anodization several different pre-treatment procedures can be applied to improve the aluminium structure as well as its surface morphology. The most widespread procedure is annealing of the aluminium in an inert atmosphere (nitrogen, argon) or in a vacuum at approximately 400 °C for at least 4 h to allow the rolled

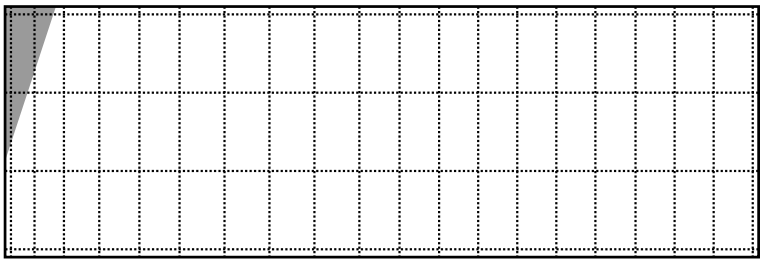

Fig. 3.2: Schematic view of top side of aluminium sample (scale 1:1). The grey part represents the manipulation part which is used for a sample contacting and holding.

structure of aluminium sheet to relax and recrystallize [17, 27]. In this work, the annealing in a vacuum or inert atmosphere was not performed due to absence of the apparatus for this type of annealing and the sample size. The annealing in general increases the grain size which naturally leads to better ordering of pores in larger areas. Despite no annealing was performed, the final results of PAA templates are remarkably good (shown in Figure 3.6 and Figure 3.11 in the result section).

In general, there are several methods to smooth a rough surface of the aluminium sheets, e.g.: mechanical, chemical or electrochemical polishing.

3.1.2 Mechanical and chemical polishing

Before mechanical polishing, sanding (by rotating sandpaper discs) was required to obtain a macroscopically flat surface. During this process, a lot of material (30-60 %) was consumed. The polishing was performed using the rotating discs with a special textile surface and using abrasive paste (abrasive particles of 3 µm size). Here, the basic issue was the fixation of the aluminium sheet during the polishing. For this purpose the aluminium sheet was fixed by glue or poly(methyl methacrylate) (PMMA) to a brushed aluminium plate. Other problems concern the sample size, which played a significant role during sanding. During this process, the aluminium sheet needs to be efficiently cooled and simultaneously the brushed material has to be washed away. This can be very difficult for large surfaces. Moreover, pure aluminium is very soft and sticky, therefore it behaves almost like glue and creates an enormous friction. Despite the fact this is the only known method capable of achieving a mirror-like surface on the aluminium sheet, it is not used anymore due to mentioned practical difficulties and the sufficient results achievable without using this technique.

Before the chemical or electrochemical polishing, it was required to clean and degrease the aluminium surface. This was done by immersing and washing the sheet sequentially into demineralized water (demi water), ethanol, acetone, and isopropyl

alcohol. The standard cleaning was done in demi water (resistance approximately 18.2 $M\Omega cm^{-1}$) and dried by the flow of clean air.

Also the native oxide layer can be dissolved in solution of NaOH. In this process, the aluminium sheet is immersed into NaOH solution (0.5 M) until small bubbles start to show up on the aluminium surface. Then it is thoroughly cleaned.

The chemical polishing is done usually in hot acidic baths, where H_3PO_4, H_2SO_4 or nitric acid (HNO_3) are used [35]. However, in this work we avoided chemical polishing. A few experiments, we have carried out, resulted in the preferable chemical solving on the grain boundaries, which leads to visualization of the grain structure. Additionally, the process became more complicated since the evolution of toxic nitrogen dioxide (NO_2) from decomposition of HNO_3 takes a place, and a highly concentrated acidic solutions at a high temperature (over 80 °C) are required.

3.1.3 Electrochemical polishing

In contrary to the previous methods, which did not result in the desired results, the electrochemical polishing in a perchloric acid solution resulted in quite good results. As already mentioned, the electrochemical polishing is in principle an anodization process during which the dissolution of the oxide is much faster than its formation. The electrochemical polishing was done in the apparatus illustrated in Figure 3.3. The difference between an electrolytic cell (Figure 1.2) is only the addition of a cooling system for maintaining the temperature. The anode (WE) in this setup was the aluminium sheet while a stainless steel mesh ($7 \times 14\,cm^2$) was used as the cathode (CE). A 1:4 by volume solution of perchloric acid (2.3M $HClO_4$) and ethanol of volume 0.6 dm^3 was used as electrolyte.

Electrochemical polishing was performed in a potentiostatic regime at 24 V. Given the fast formation and dissolution of the oxide layer the electric power requirements are very high for this process. It was observed, that at the beginning of the electrochemical polishing, the current density rose to 300 $mAcm^{-2}$. After a few seconds it decreased to the steady-state value of 40 $mAcm^{-2}$. To lower the overall current flow as well as power requirements for the power supply (Matrix MPS 3020) and the cooling system, the bottom side of the sheet was covered by resist (PMMA) or sticky tape, to prevent its polishing.

Nevertheless, powerful cooling was applied to compensate for a relatively high (1.2 A) current flow through the electrolyte. The electrolyte was vigorously stirred and cooled by a system of double-walled glass and thermoregulation (Hubert - Petite Fleur/K20) to below 5 °C. The temperature of electrolyte was monitored by thermometer, while the temperature of the cooling liquid (silicon oil) was set by the thermal regulation. The low temperature (below 10 °C) is required for uniform

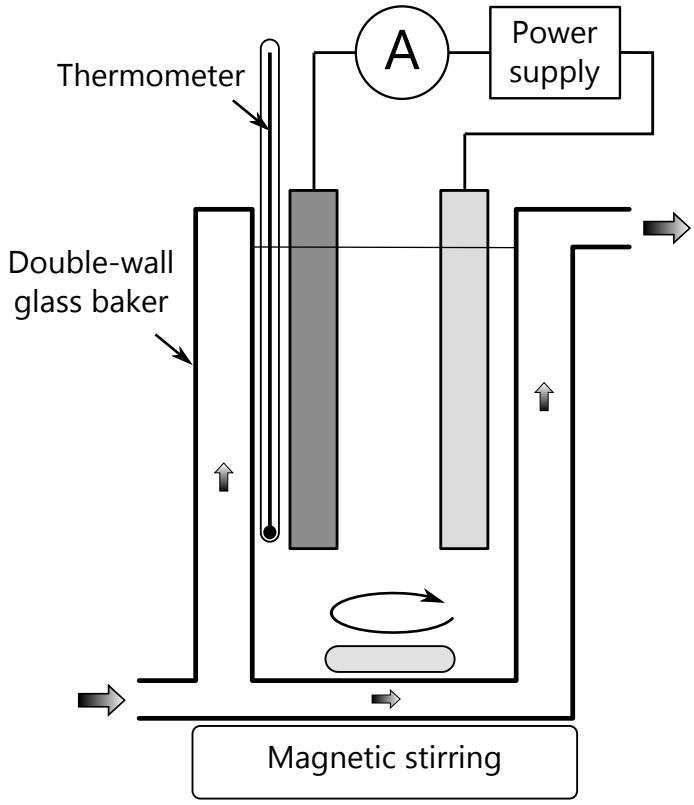

Fig. 3.3: The schematic illustration of the electrochemical polishing and anodization apparatus.

polishing without local burning due to thermally enhanced dissolution. Thanks to the powerful cooling system, the temperature of the electrolyte increased only by 1–2 °C during the process.

The time of polishing was approximately 2 min. This process is characterized by the formation of a grey layer during the first few seconds. This layer is subsequently peeled off by vigorous stirring and after that a shiny aluminium surface is revealed. It was observed that longer polishing times resulted in a more mirror-like effect, and thus a smoother surface. After polishing, the sample was cleaned in the standard fashion as described in subsection 3.1.1.

3.2 Anodization

The aim of the anodization process was a fabrication of PAA with a thickness of approximately 50 µm and a pore diameter of 40–50 nm. These parameters were chosen as the most suitable for the experimental study of the electrochemical deposition of nanowires. While the thickness was primarily chosen based on the manipulation requirements, because the required length of nanowires is less than 1 µm, the pore

diameter was chosen in respect to the properties of nanowires. The pore diameter of approximately 50 nm was chosen as the most suitable for the SEM as well as an eventual optical characterization. Moreover, the anodization in oxalic acid (40–90 nm) has been the most studied method and showed a greater reproducibility than anodization in sulfuric acid (less than 25 nm) and phosphoric acid (larger than 120 nm).

The well-known two-step anodization (see schematic diagram in Figure 3.4) under standard conditions [36] has been used for the fabrication of PAA with well ordered pores. Despite the fact that a well-ordered PAA with the thickness of tens of micrometres (from the bottom) is easily achievable by the long one-step anodization, the two-step anodization was chosen for two reasons. The first minor reason is to fabricate the perfect and uniform PAA through its whole thickness. The second practical reason is based on the restriction of the anodized surface by the resist (PMMA). This will be explained during the description of the procedure.

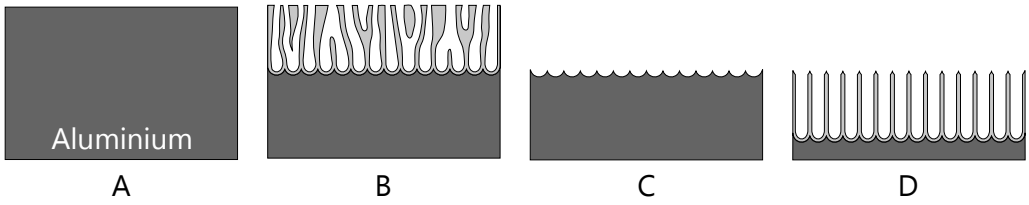

Fig. 3.4: Schematic diagram of the two-step anodization. Polished aluminium sheet (A) is anodized, which results in a formation of the hexagonally ordered PAA layer with thin disordered top layer (B). After removal of the PAA, the aluminium surface retains the hexagonally ordered pits created by the bottom side of the honeycomb structure (C). The second step of anodization leads into formation of ordered PAA without a disordered layer (D).

The anodization apparatus is illustrated in Figure 3.3. The cooling system was the same as in the electrochemical polishing process. The power supply (Agilent 6645A#J05) and ammeter (Agilent 34970A Data Acquisition/Switch Unit with Agilent 34901A) were controlled by a computer. The solution of 0.3M oxalic acid of volume 0.6 dm^3 cooled to 7 °C was used as electrolyte. The first step of anodization took 14 h (50 µm) to ensure a very good pore ordering at the bottom of the PAA. After the anodization of the entire surface, the bottom side and the edges of aluminium sheet were covered by the resist (PMMA) to define the anodization area (shown in Figure 3.5B). It is important to apply resist on the PAA layer because in case of a direct application on the aluminium surface, it will likely peel off during the second anodization. This usually leads to an undesirable anodization of the aluminium under the resist layer which results in undefined anodization and it

complicates the removal of the aluminium substrate.

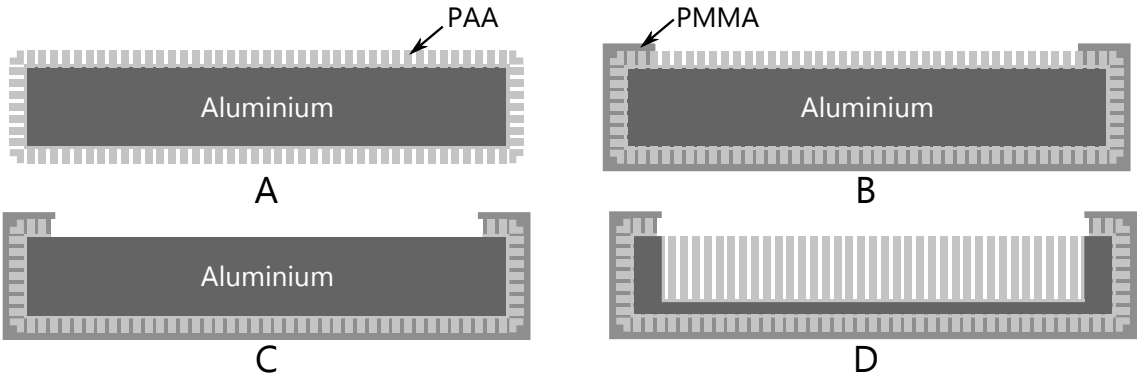

Fig. 3.5: Schematic diagram of the experimental realization of two-step anodization and resist application. On the anodized aluminium sheet (A) is applied the PMMA mask (B) which define anodization area for the second step. After that, the uncovered PAA layer is removed to obtain the well-ordered pre-patterned aluminium surface (C). Subsequently, the second anodization leads into formation of the uniform PAA layer (D).

In this work PMMA is frequently used as an isolation layer. For this purpose solid PMMA was dissolved in anisole. Various concentrations (viscosities) were used in respect to applications and the desired thickness of the resist layer. This process consists of manually coating a thick layer (thicker than 5 µm) over a sample and baking it on a hotplate for one minute at approximately 145 °C (the boiling point of anisole is 154 °C).

After application of the resist layer, the procedure continued with the etching of the uncovered PAA layer to achieve the pre-patterned aluminium surface (Figure 3.4C and Figure 3.5C). This process was done by chemical etching in a mixture ($0.2\,dm^3$) of 0.75M H_3PO_4 and 0.3M chromium trioxide (CrO_3) for 30 min at 55 °C. Because of the high toxicity of Cr^{VI+} the sample needs to be washed properly. The resulting aluminium surface is shown in Figure 3.6. In Figure 3.6 (left), the influence of the grain structure of aluminium can be seen. This leads to small defects in the perfect hexagonal order, e.g. mutual rotation of the grain pore structure and minor defects on the grain boundaries.

The second step of the anodization was conducted at the same conditions as the first step (40 V, 0.3M oxalic acid, 7 °C, 14 h) to match the pre-patterned aluminium lattice and obtain uniform pores (Figure 3.4D and Figure 3.5D).

However, some experiments were done using the Keithley 2400 SourceMeter as a power supply which resulted in a different structure of the top PAA layer (shown in Figure 3.7). This difference is specifically caused by the different current limit of each device. The top view of PAA formed by anodization at 40 V with current limit

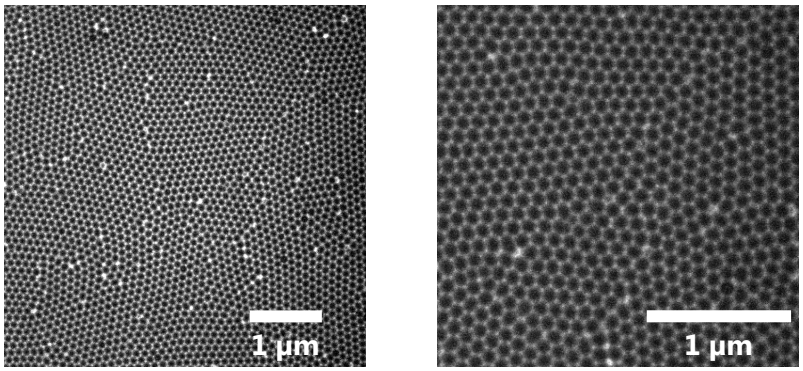

Fig. 3.6: The SEM images of aluminium surface after the first step of two-step anodization (40 V, 14 h, 7 °C).

of 1 A (Agilent 6645A#J05) and 105 mA (Keithley 2400 SourceMeter) is shown in Figure 3.7(left) and Figure 3.7(right), respectively. Regardless the pore order, the

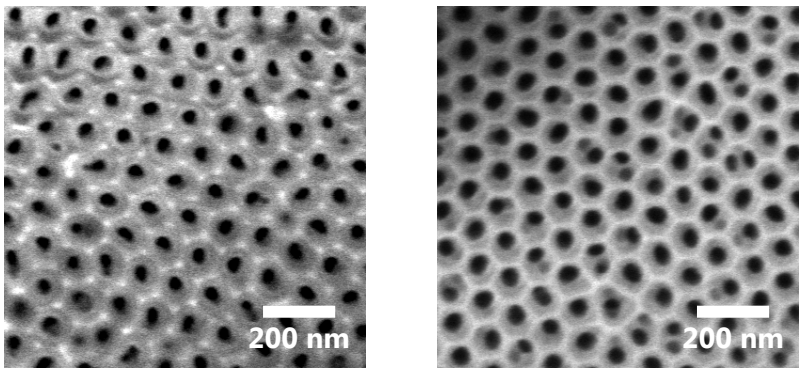

Fig. 3.7: The top view (SEM) of the PAA formed by two-step anodization at 40 V (14 h, 7 °C) with current limit of 1 A (left) and 105 mA (right).

nucleation of one pore inside one pit can be seen in Figure 3.7, however two or more pores occasionally appear inside one pit in Figure 3.7(right). The origin of this effect is in the high current density at the beginning of the anodization, caused by the large surface area of aluminium and its low resistance. The ideal kinetics of PAA growth in potentiostatic regime are shown in Figure 2.3B. However, now the current density (current) is limited by the power supply. The experimental relationships of anodization current and voltage are shown for current limit of 105 mA in Figure 3.8. Here, it can be seen that the process is divided into the galvanostatic regime (first 1.2 min) and the potentiostatic regime. It is expected that during the galvanostatic regime the anodizing potential was lower than the required one (40 V), thus the potential corresponding to the pre-patterned structure. This leads into nucleation of smaller pores corresponding to the lower anodizing voltage, resulting in the final structure shown in Figure 3.7(right).

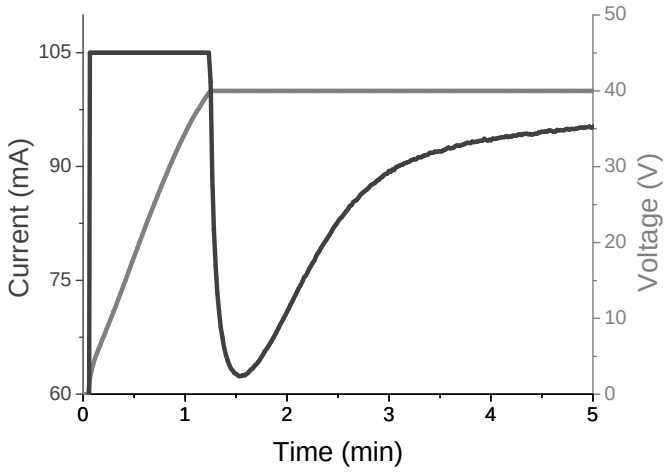

Fig. 3.8: The measured relationship of anodization voltage and current during early stage of second anodization at 40 V ($\approx 30\,\mathrm{cm}^2$, 7 °C) with current limit of 105 mA.

Also, it is necessary to emphasize that the top view gives us only partial information about pore size. Despite the fact that the initial pore diameter depends on many factors (surface, voltage, etc.), it is always smaller than pore diameter of the steady-state growth (illustrated in Figure 2.3C stage c).

3.3 Modification of Porous Alumina

From the previous steps we have obtained the PAA layer on the aluminium substrate (Figure 3.1E) with a resist layer. However, due to the insulating barrier layer PAA is not open-through, thus the electrochemical deposition within this system (PAA on the aluminium substrate) is nearly impossible.

The removal or the penetration of the barrier layer is one of the fundamental issues in the use of PAA as the template for the electrochemical deposition. One of the most promising approaches concerning the anodization of valve metals will be discussed in the end of this chapter in section 3.5. Alternatively, the use of continual decrease of the anodizing voltage (or current) results in a thinner barrier layer [37]. The subsequent chemical etching of the PAA can be used to remove residual barrier layer and to widen the pores [38,39]. However, this also results in pore branching at the bottom of the PAA which is undesirable for the fabrication of uniform nanowires. This can be overcome by the electrochemical etching of the barrier layer which was proposed by various scientific groups (e.g.: [40, 41]). These techniques were studied but not adequately verified to present any valid conclusions. Nevertheless, we focus on the chemical etching of barrier layer which is described in the next subsection.

3.3.1 Preparation of open-through porous alumina

Because the barrier layer has approximately the same composition as the rest of the PAA, it is important to expose only the barrier layer to the etching solution, while the time of the etching needs to by precisely controlled to etch only the barrier layer without additional pore widening, if it is not desirable.

To achieve this, the procedure illustrated and described in Figure 3.9 was carried out. The chemical etching of the covering PAA was done in same way as the etching

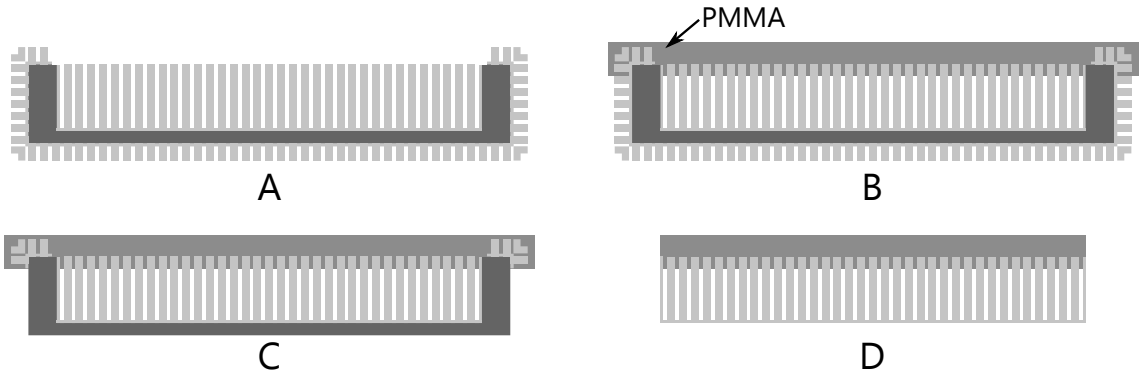

Fig. 3.9: Schematic diagram of the experimental preparation of PAA before chemical etching of the barrier layer. At first, the sample was thoroughly rinsed in acetone to remove the PMMA layer (A). After that, the layer of PMMA was applied on the top side to cover the prepared PAA (B). Then PAA formed by the first step of the anodization was removed (C) and finally the aluminium substrate was removed by chemical etching, leaving the barrier layer exposed (D).

in the two-step anodization process (etching solution: 0.75M H_3PO_4 and 0.3M CrO_3, 30 min at 55 °C). After, the sample was properly washed in the demi water; the aluminium etching was done in solution of 6M hydrochloric acid (HCl) and 0.3M copper(II) chloride ($CuCl_2$) of volume 0.2 dm^3. The etching time depends on the thickness of residual aluminium and it usually takes 1 h. After this procedure, we obtained the PAA film of thickness 50 µm covered by PMMA with an exposed barrier layer (shown in Figure 3.10). Without the aluminium substrate the PAA becomes very fragile, thus it needs to be carefully handled.

We have studied the etching of the barrier layer in 10% H_3PO_4 (1.73M) at 50 °C [42]. The etching rate of the barrier layer has been found, specifically 10 and 16 nm per minute for barrier layer formed in oxalic acid and sulfuric acid, respectively. However, in this work we used etching solution (0.75M H_3PO_4 and 0.3M CrO_3) at 55 °C instead, which has approximately the same etching rate as 10% H_3PO_4 at 50 °C. Because the barrier thickness differed slightly for samples prepared by the same procedure, the etching time could not be precisely determined.

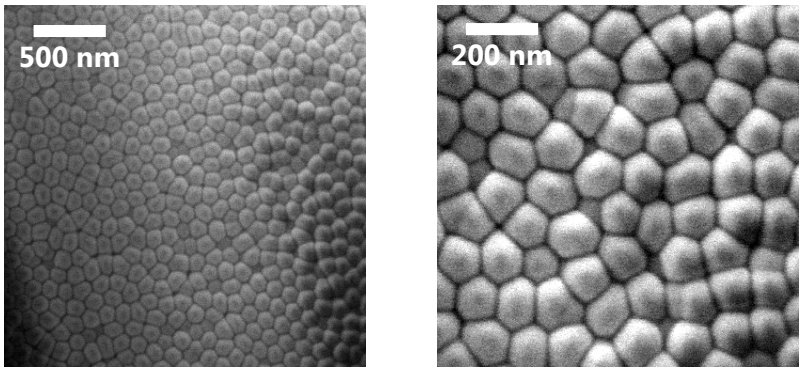

Fig. 3.10: The bottom view (SEM) of the barrier layer formed by two-step anodization at 40 V (14 h, 7 °C) and exposed by the etching of the aluminium substrate. (The disordered structure is specific for this sample.)

The reason for the formation of different barrier thickness is probably influenced by the time which the samples spent in the electrolyte after anodization ends. Because the anodization takes 14 h it is performed over night while the power supply is controlled by a computer. Thus, when the anodization ends the power supply is turned off and the sample needs to be manually taken out of the electrolyte. This requires a good time schedule which was not always followed.

The advantage of the etching solution (with CrO_3) is its intense red colour which helps to distinguish between stages of the barrier etching. When PAA is rinsed into the etching solution it is like a glass. After few minutes (2–3 min) it becomes milky white. Then, approximately at the 4th minute of etching, the PAA becomes crystal clear which corresponds to penetration of the barrier layer and pores' filling. The etching time depends on the barrier thickness, concentration and temperature of the etching solution. A few results are shown in Figure 3.11 (bottom views) and Figure 3.12 (cross section).

This step concludes whole process of the PAA fabrication, even though the top side of the PAA is still covered by PMMA, this layer will be removed after the deposition of the working electrode.

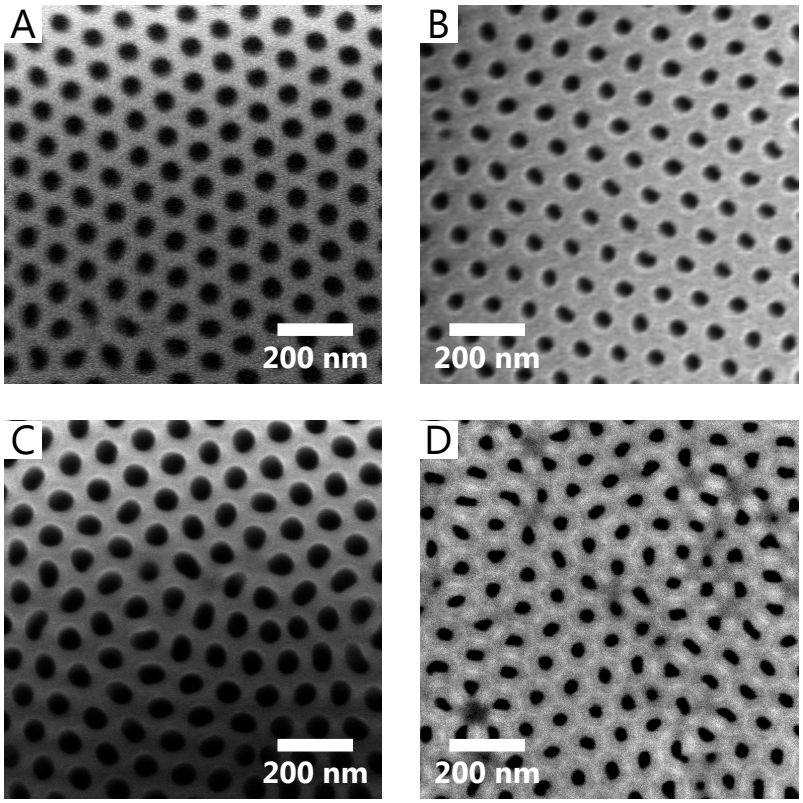

Fig. 3.11: The bottom view (SEM) of various PAAs fabricated by discussed procedure after removal of the barrier layer. The pore diameter is 50 nm (A), 42 nm (B), 54 nm (C), and 34 nm (D).

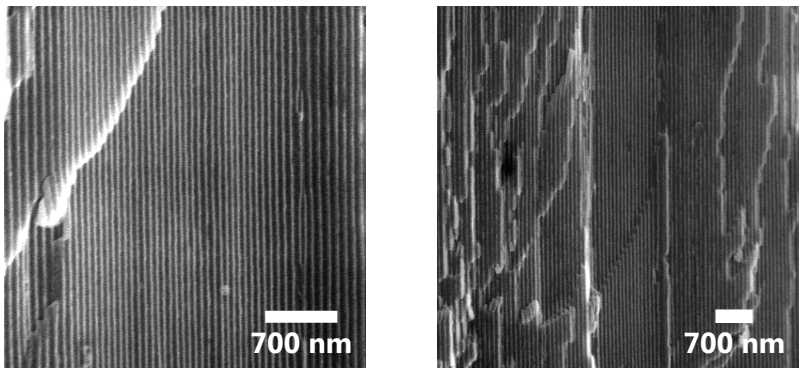

Fig. 3.12: The cross section (SEM) of the PAA for which the bottom view is shown in Figure 3.11A.

3.3.2 Deposition of the working electrode

Deposition of the working electrode (WE) using the physical vapour deposition (PVD), was done by specialists (and not the author of this work), thus further discussion is focused only on the resulting layer. Various methods were studied:

magnetron sputtering at the Institute of Materials Science and Engineering, ion beam sputtering in the Institute of Physical Engineering and evaporation deposition in the laboratory of LabSensNano. Because of the large sample size the evaporation methodproved to be the best solution.

The main requirements on the layer were: smoothness and continuity (compactness), and chemical inertness during electrochemical deposition from various electrolytes. Based on the availability of the materials (Pt, Au, Ag), gold was chosen as the material of the WE. This choice brings the expected problem of the gold nanowires separation from the WE, which will be discussed in chapter 4 in detail.

Various gold layers were obtained; the best one was the deposited layer of the thickness 250 nm shown in Figure 3.13. Despite the fact that deposition details are not available, it is expected from the large grains that the evaporation rate was very fast. This fast deposition partially nullifies a problem with pore filling by the deposited material. On the other hand, slow deposition leads to a fine smooth layer shown in Figure 3.14(1c) and Figure 3.14(1b). Figure 3.14(1c) shows the filling effect of the pores. This effect can be reduced by an increase of the deposition rate or the deposition angle. Figure 3.14(1b) present the porous character of the deposited gold layer which is primarily caused by its small thickness (150 nm). Even though that the relationship between the resulting layer on the PAA, deposition rate, and thickness of deposited layer was not studied, it is assumed that a thinner layer is needed to enclose pores at a higher deposition rate than at a lower deposition rate.

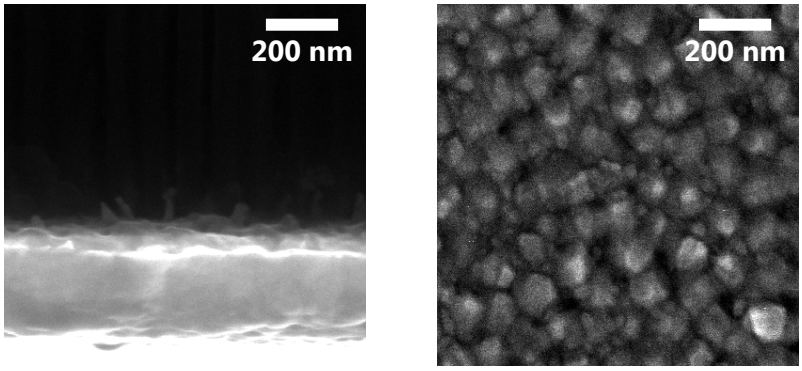

Fig. 3.13: The SEM image of the evaporated gold layer of thickness 250 nm on the bottom of the PAA: cross section (left), bottom view (right).

Firstly, it was assumed that the porous structure of WE would not play an important role during the electrochemical deposition, especially if it will be covered by the resist layer afterwards. However, it was found that this assumption was wrong. Thus, the need for creating compact gold layer grew in importance. Additionally, problems with the deposition of the thick gold layer and a large consumption of the material led to a development of a post-treatment method of porous gold layer.

For this purpose we have studied various annealing procedures (temperature, time) of the porous gold layer on the PAA in ambient atmosphere. Before annealing, the PMMA layer from the previous step was removed by immersing and washing the PAA in acetone. Annealing at 300 °C for 10 min was found as the most suitable, leading to a compact layer (Figure 3.14(2b)) and removal of gold from the pores (Figure 3.14(2c)). Since the annealing leads to the major improvement of the layer quality, all samples were annealed before the electrochemical deposition of nanowires. The only notable drawback of this step is in the increased fragility of the PAA, probably caused by a change of the structure and its chemical composition.

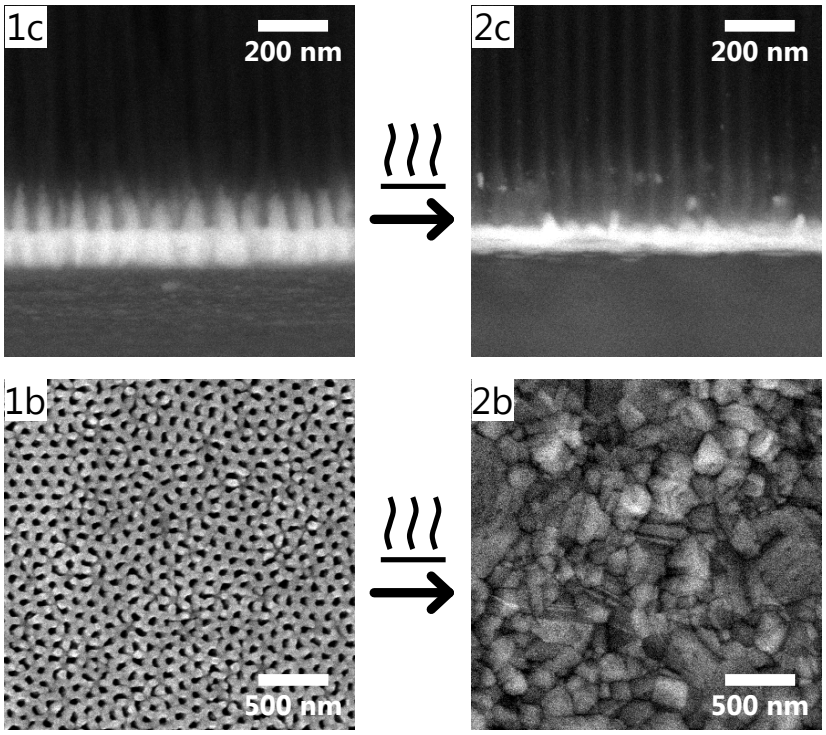

Fig. 3.14: The SEM images (cross section (1c), bottom view (1b)) of the evaporated gold layer of thickness 150 nm on the bottom of the PAA. This layer was annealed in ambient atmosphere at 300 °C for 10 min which resulted in the layer shown in cross section (2c) and bottom view (2b).

3.4 Fabrication of Gold Nanoparticle Array

In this section, we describe the preparation of the ordered array of gold nanoparticles by a very simple method. This research was proposed on the basis of the results from the annealing of the gold layer (WE). Because it is not in the primary objectives of this work, the potential of this method has not been more developed than it

is presented. However, outstanding results and simplicity of the whole fabrication procedure are the main advantages which would motivate a further study.

This method employs the well-known dewetting effect of the annealed gold layer [43,44]. As a substrate we have used the pre-patterned aluminium surface created by the first step of the two-step anodization (Figure 3.6). This method is schematically illustrated in Figure 3.15.

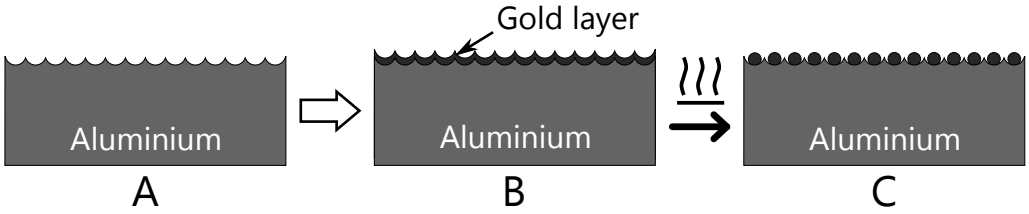

Fig. 3.15: Schematic illustration of the nanoparticle fabrication method. On the pre-patterned aluminium surface (A) a very thin layer of gold is deposited (B) which is then annealed (C).

Within this work we have studied the relationship of the final particles size on two kinds of aluminium surface structures. The structure formed by anodization at 40 V in oxalic acid was covered by 15 nm thick gold layer (sputtered) and annealed in ambient atmosphere at 250 °C for 90 min. This results in the uniformly distributed gold particle size of 73 nm (shown in Figure 3.16(left)). Another type of surface

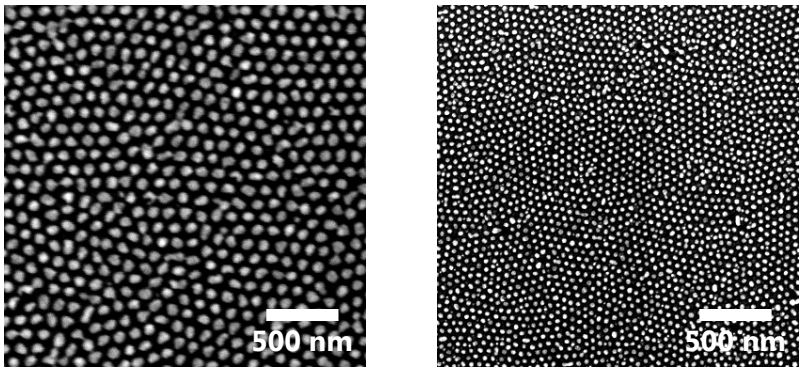

Fig. 3.16: The SEM images of the gold particles formed by the annealing of the gold layer on the pre-patterned aluminium surface. The particle size of 73 nm (left) and 35 nm (right) for aluminium surface formed by the anodization at 40 V (oxalic acid) and 20 V (sulfuric acid), respectively.

was prepared by anodization in the sulfuric acid at 20 V, covered by 6 nm thick gold layer and annealed in an ambient atmosphere at 300 °C for 90 min, and resulted in the particle size of 35 nm (shown in Figure 3.16(right)).

Additional relationship between particle structure and the thickness of the gold layer, temperature of the annealing, thickness of the native aluminium oxide, were briefly studied. However, more extensive experimental work is required in this area to be able to propose any reliable conclusions.

3.5 Thin Layer Technique

It would be inappropriate not to mention the fabrication of the PAA by thin layer technique; even through it was not widely used within this work. The main difference between the procedure described above and this technique is the starting material: a thin layer (hundreds of nanometers) of aluminium (sputtered, evaporated, etc.) on a substrate (silicon wafer, glass). Thus, given by this configuration, a lot of advantages and problems can be expected.

First, the properties of the aluminium layer can by precisely controlled. This includes the layer thickness, its composition, surface morphology, as well as the crystal structure of the layer. The main benefit of this method are possible applications of the PAA as a mask or a template on various substrates. Additionally, one of the promising applications, is a potential implementation within integrated circuits, sensors, etc.

On the other hand, the drawback of this technique is the thin aluminium layer which is inadequate for two-step anodization. Thus, for obtaining of a well-ordered PAA structure, it is necessary to pre-pattern the aluminium surface by some other method like mould imprinting. Moreover, the removal of the barrier layer becomes the main issue. The worldwide scientific efforts to solve this problem has resulted in the development of many techniques. One of the most convenient is the use of an intermediate layer consisting of a valve metal (Ti, W, Zr, Ta, Nb, etc.) under the aluminium layer. This leads to the anodization of the intermediate layer, e.g. tungsten layer, which results in a penetration of the barrier layer by the structures of tungsten trioxide (WO_3) (shown in Figure 3.17B). The subsequent selective chemical dissolution of the WO_3 structures results in open-through PAA suitable for electrochemical deposition (Figure 3.17C). It is expected that different anodization times of the intermediate layer can form various structures, and thus good control is required [45].

For the anodization of the wafer it is generally required to use a special anodizing cell, where only a part of the surface is exposed to the electrolyte. The schematic illustration of one possible design of the anodizing cells used and developed in the laboratory of LabSensNano is shown in Figure 3.18. The anodizing area is usually a circle with diameter of 5 mm. The cooled electrolyte circulation and cooling plate

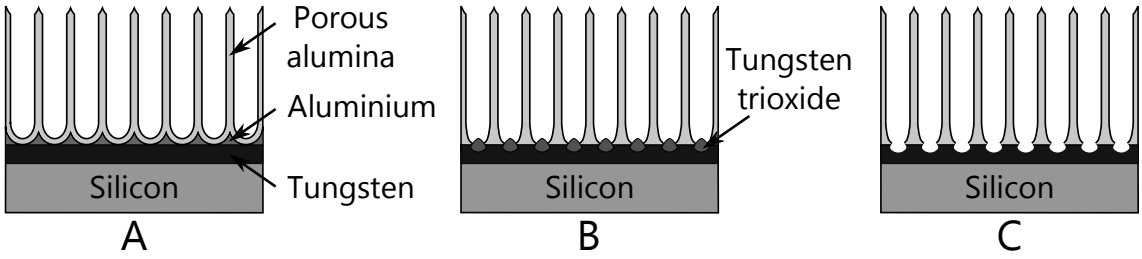

Fig. 3.17: Schematic illustration of the fabrication of open-through PAA on the wafer.

ensure stable concentration and temperature of the electrolyte. To overcome the

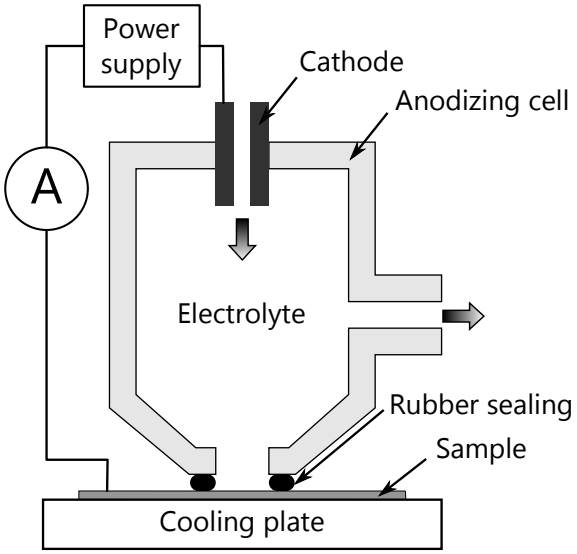

Fig. 3.18: Schematic illustration of the anodizing cell for the thin layer anodization used and developed in laboratory of LabSensNano.

drawback of the small anodizing area and complicated setup, the wafer was covered by a resist (PMMA) and anodized in the standard anodizing apparatus (Figure 3.3). Despite a great effort to insulate the wafer by the thick resist layer, undesirable anodization of silicon could not be avoided in our work. Additionally, due to a shortage of samples, most of the attention was focused on the anodization of the aluminium sheets.

As a result, all electrochemical depositions were done within the templates fabricated by anodization of the aluminium sheets, described in the previous sections. The electrochemical depositions as well as their results are presented in the next chapter.

4 ELECTROCHEMICAL DEPOSITIONS

In this chapter, we discuss the methods used for electrochemical deposition within the PAA templates and present the achieved results.

4.1 Experimental setup

The experiments were done in a simple two-electrode cell apparatus with a stainless steel sheet ($2\times6\,\mathrm{cm}^2$) as the CE and the PAA with a gold layer as the WE. These electrodes were connected (four-terminal sensing) to the power supply (Keithley 2400 SourceMeter), which was controlled by a computer. An electrolyte of volume $0.1\,\mathrm{dm}^3$ at room temperature was gently stirred.

A method using a printed board for better fixation of PAA templates in a standard electrical clip (illustrated in Figure 4.1) was proposed and tested. The idea consisted of PAA fixation by double sided adhesive copper tape or colloidal silver (dissolved in anisole) on the conductive part of the printed board in order to achieve good support. An insulation was done by the application of PMMA. Finally, the right-half of the printed board was dipped into an electrolyte while the left part was used as a connecting area.

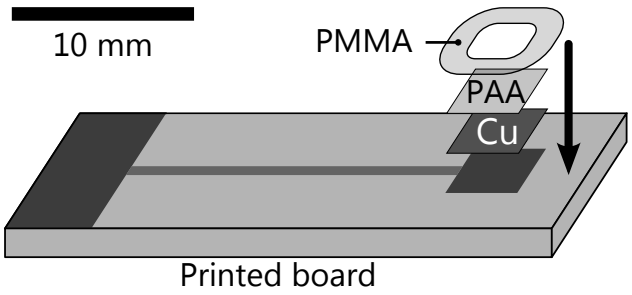

Fig. 4.1: Schematic illustration of the printed board method of PAA fixation for electrochemical deposition.

However, this setup frequently resulted in the etching of the PAA, oxidation or dissolution of the copper tape, and other undesirable effects taking place during deposition. The hypothesized reason is a defective gold layer caused by the fixation (due to weak adhesion of the gold layer to PAA) or by the gold layer deposition itself. Additionally, complications with the fixation and especially removal of PAA from the printed board resulted in a development of an even simpler method.

This method is illustrated in Figure 4.2. At first, a strip of adhesive copper tape was attached to the bottom (for electrical contact) and the top of PAA. Then the PAA template was covered by PMMA from the bottom side and partially the top

side (to define the WE area) as it is illustrated in Figure 4.2. The soft strip of copper tape was used as a connection area for an electric clip while the covered part of the template has been dipped into the electrolyte.

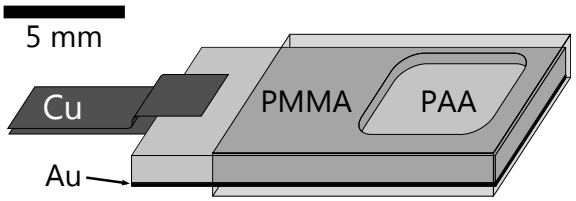

Fig. 4.2: Schematic illustration of the PAA preparation for the electrochemical deposition. The sample is vertically half dipped into the electrolyte to only expose the PAA area defined by PMMA.

Even though this method is very suitable for experimental purposes, it has a few drawbacks. The main issue is a lack of support for the fragile PAA template, due to which 10–20 % of samples were broken by manipulation. Another issue is connected with the manual application of PMMA which results in varying and poorly defined areas of PAA being exposed to the electrolyte. However, an enormous advantage is that the template does not need any special treatment (like removal of PMMA) before the SEM characterization.

4.2 Electrochemical Deposition of Materials

At the beginning of this section, it is required to describe and understand the measurement method used in the fabrication process of nanowires. The origin of the primary measurement error is in the measurement of PAA area within which the deposition occurs. Because this area is defined by the PMMA layer, which is applied by hand, it is very irregular and varies for each sample. Since no sophisticated methods for the area measurement were applied, the measurement error of this measurement is estimated in the range of 10–25 %.

The systematic error of the estimation of deposition time is ± 1 s (0.3–10 %). The current and the voltage are measured with a measurement error of less than 0.5 %, thus we can neglect these errors.

The measurements of length of nanowires were done by SEM as discussed in appendix A.

Because the sample size is not well defined, the galvanostatic depositions were done with a constant current for a set of samples. The current densities, reported in this chapter, were subsequently calculated in respect to the sample area, thus they are very approximate and more or less illustrative. In the following text, we

will refer to potentiostatic or galvanostatic deposition presenting only voltage or current density, respectively. The voltage values represent the absolute value of the potential difference between the WE and the CE, as set and measured by a power supply (Keithley 2400 SourceMeter). Thus, we use positive values for the reduction (Au, Ni, etc.) as well as the oxidation process (PANI).

4.2.1 Electrolytes and materials of deposition

Because the main goal of this work was the fabrication of the Au-PANI-Au NW structure (illustrated in Figure 1), the deposition of gold and polyaniline became the primary subject of this experimental study. However, due to the initial problems with the deposition and especially the SEM characterization of PANI nanowires, we have looked for alternatives. The first possible substitution for PANI was a nickel interlayer, for which the electrical conductivity can be modified by a post-process thermal oxidation [4]. Additionally, the depositions of chromium, silver, and copper were studied.

All materials were deposited from individual electrolytes specific for each of them. The aqueous electrolytes studied in this work are listed below:

Gold

Cyanide bath: 0.02M $K[Au(CN)_2]$, 0.4M H_3BO_3.

Non-cyanide bath: 0.025M $HAuCl_4$, 0.42M Na_2SO_3, 0.42M $Na_2S_2O_3$ [46, 47].

Nickel

Standard Watts bath: 1M $NiSO_4 \cdot 6\,H_2O$, 0.2M $NiCl_2 \cdot 6\,H_2O$, 0.5M H_3BO_3.

Polyaniline

0.1–0.5M aniline, 0.2–0.5M H_2SO_4, (or 0.3M $HClO_4$).

Copper

0.2M $CuSO_4 \cdot 5\,H_2O$, 0.2M H_2SO_4, 0.1M H_3BO_3.

Chromium

2.5M CrO_3, 0.025M H_2SO_4.

Silver

0.05M $AgNO_3$, 0.3M H_3BO_3, (and 0.5M H_2SO_4).

Despite each electrolyte having a different composition, they are all very similar. The main component of an electrolyte is the ion source (e.g.: $K[Au(CN)_2]$, $CuSO_4 \cdot 5\,H_2O$) which is usually a salt of the deposited material. Additional components can serve as pH buffers (e.g., H_3BO_3) or can increase the electrical conductivity of the electrolyte (e.g., H_2SO_4), or even influence the structure of the deposited material.

4.2.2 Deposition of films

Before deposition within the PAA templates, each deposition was first tested in a setup where a stainless steel sheet covered by PMMA with the exposed area of approximately $1 \times 1\,\mathrm{cm}^2$ was used as the WE. Depositions were conducted in a galvanostatic regime with the current density over $5\,\mathrm{mAcm}^{-2}$ and they were terminated after a macroscopically compact and thick layer was formed. The deposition of gold and copper resulted in a compact and matte layer with low adhesion to the substrate. On the other hand, nickel and chromium ($25\,\mathrm{mAcm}^{-2}$) formed a very thick layer with high adhesion. Unfortunately, the silver deposition did not form any visible layer.

Apart from that, the most interesting results were from the deposition of PANI. During deposition, a blue layer was formed on the surface. When the current density was intentionally decreased during reaction, the blue deposited layer changed its colour to green. It is assumed that this change is in the relationship with the PANI protonation by an acidic electrolyte. Thus, the lower deposition rate leads to formation of an electrically more conductive form of PANI. Also, it was observed that after the formation of a thin compact layer, additional PANI has been flushed out into an electrolyte, resulting in a finite thickness of the PANI layer, regardless of the time of deposition. However, this fact was not studied in detail because the created layer of PANI appeared to be few micrometres thick which is enough for use in the Au-PANI-Au nanowires. Additionally, the protonation in an acidic solution (1.73M H_3PO_4) and the deprotonation in an alkaline solution (0.5M NaOH) of the PANI layer, accompanied by colour change from green to blue and vice versa was performed and observed.

4.2.3 Au-PANI-Au nanowires

While the previous section's experiments immediately resulted in good compact layers without any significant adjustments of the deposition parameters, the deposition within the templates proved to be more complicated.

Firstly, it was found that deposition of any listed material is not possible within the templates which have a porous gold layer (WE). This includes templates fixed by the adhesive copper tape or the colloid silver on the printed board (Figure 4.1) as well as the templates covered by PMMA (Figure 4.2). The deposition of gold resulted in PAA etching for templates fixed by the colloid silver (Figure 4.3(right)) as well as templates fixed by the adhesive copper tape (Figure 4.3(left)). While in the first case the gold layer remained on the PAA, in the second case the gold layer completely detached which was caused by the adhesive tape or the etching process. In both cases of the SEM characterization, the templates were detached

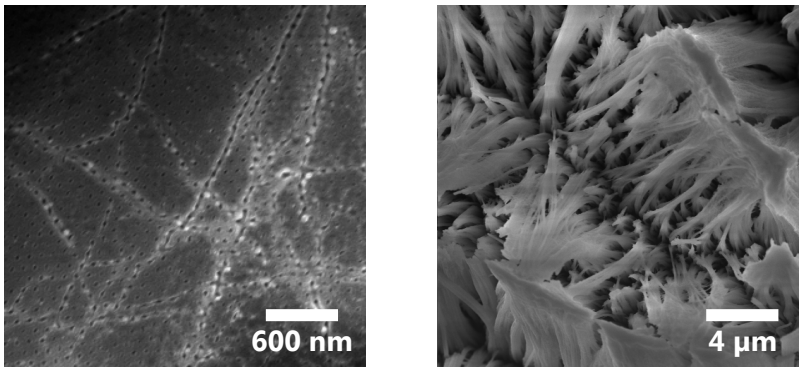

Fig. 4.3: The SEM images (bottom view) of the PAA templates fixed on the printed board after unsuccessful gold deposition.

from a printed board by chemical dissolution in acetone. Even though the nature of this process is not fully understood, it is assumed that due to the complicated system of multi electrode/electrolyte interfaces (electrolyte/gold/electrolyte/copper tape or silver), various processes can occur.

Moreover, covering of the template with porous gold layer by PMMA (Figure 4.2) results into either PAA etching or the situation in which no current flows as the pores are blocked by the resist. Until this problem was solved by using the annealing step, it had been overcame by the deposition within templates without the resist layer. This resulted in the deposition of material within the template, forming a nanowire array as well as the deposition from the bottom side of the WE, forming a macroscopically compact layer. This method has not been used for further experiments inter alia, due to the increased material consumption.

After solving the problem with the templates, we focused on the deposition of simple PANI nanowires. A lot of experiments that were done resulted in a good macroscopically homogenous coverage. Moreover, the part of the template within which PANI was deposited, changed its colour in acidic and alkaline solution in the same way as the PANI layer. However, the characterization of a cross section by the SEM did not provide any evidence of nanowire growth. Thus, after a great struggle, we assumed that this is caused by poor contrast of PANI in the PAA matrix. This problem was also studied in the work [48] where authors used the silver and copper segments as a marker for the PANI nanowires. Therefore, to observe the PANI nanowires, the template was fixed by the PMMA on a ceramic plate (the bottom down) and the PAA was dissolved in 0.5M NaOH for 2 h. Demonstrational results obtained by this procedure are shown in Figure 4.4. Based on this, we assumed for further nanowire characterization that PANI appears invisible in contrast with the PAA template. All presented results of the PANI nanowires were obtained by deposition from the 0.3M aniline and 0.5M H_2SO_4 solution. To achieve higher

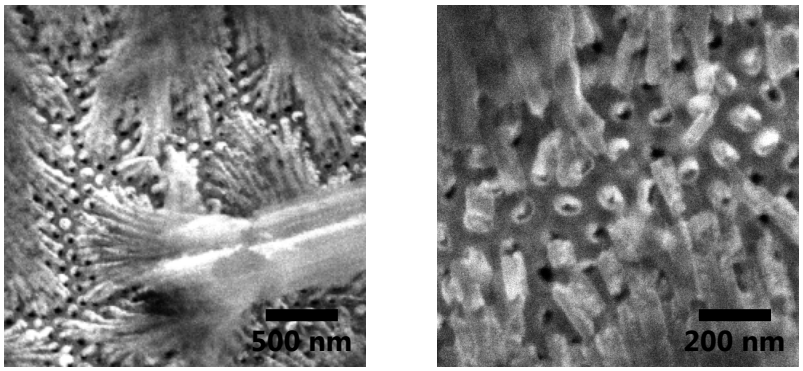

Fig. 4.4: The SEM images (top view) of PANI nanowires on gold substrate layer after removal of PAA template.

electrical conductivity of the PANI, the deposition was conducted at a low current density (0.4–2 $\mathrm{mAcm^{-2}}$) or the corresponding voltage of 0.9 V.

Since the deposition of PANI nanowires proved to be successful, we focused on the gold nanowire deposition. In this work, we studied the deposition of gold from the cyanide bath (0.02M $K[Au(CN)_2]$, 0.4M H_3BO_3) at room temperature (RT, approx. 23 °C) and at a higher temperature of 60 °C. In summary, the deposition at RT proved to be more suitable because the cyanide bath at 60 °C etched the PMMA which resulted in uncontrolled deposition. Additionally, the SEM characterization of gold nanowires deposited at 60 °C and RT did not show significant differences. The results of the combined depositions of the Au-PANI-Au segments are shown in Figure 4.5 and Figure 4.6. Between the individual depositions, the sample was

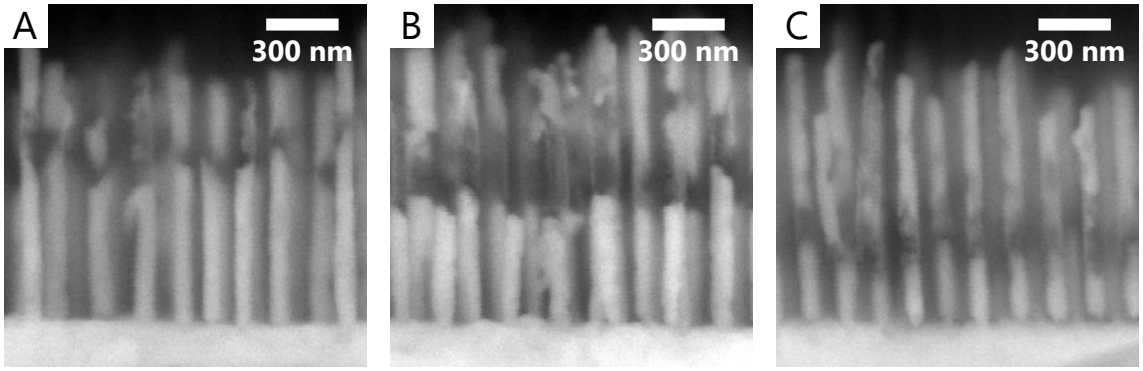

Fig. 4.5: The SEM images (cross section) of Au-PANI-Au nanowires deposited at various conditions. (A): Au, 0.45 $\mathrm{mAcm^{-2}}$, 60 °C, 300 s; PANI, 0.9 V, 250 s; Au, 0.45 $\mathrm{mAcm^{-2}}$, 150 s. (B): Au, 0.63 $\mathrm{mAcm^{-2}}$, 150 s; PANI, 0.9 V, 250 s; Au, 0.63 $\mathrm{mAcm^{-2}}$, 150 s. (C): Au, 2 V, 330 s; PANI, 0.9 V, 100 s; Au, 0.83 $\mathrm{mAcm^{-2}}$, 150 s.

cleaned using standard techniques. In the images (Figure 4.5), we can see that the

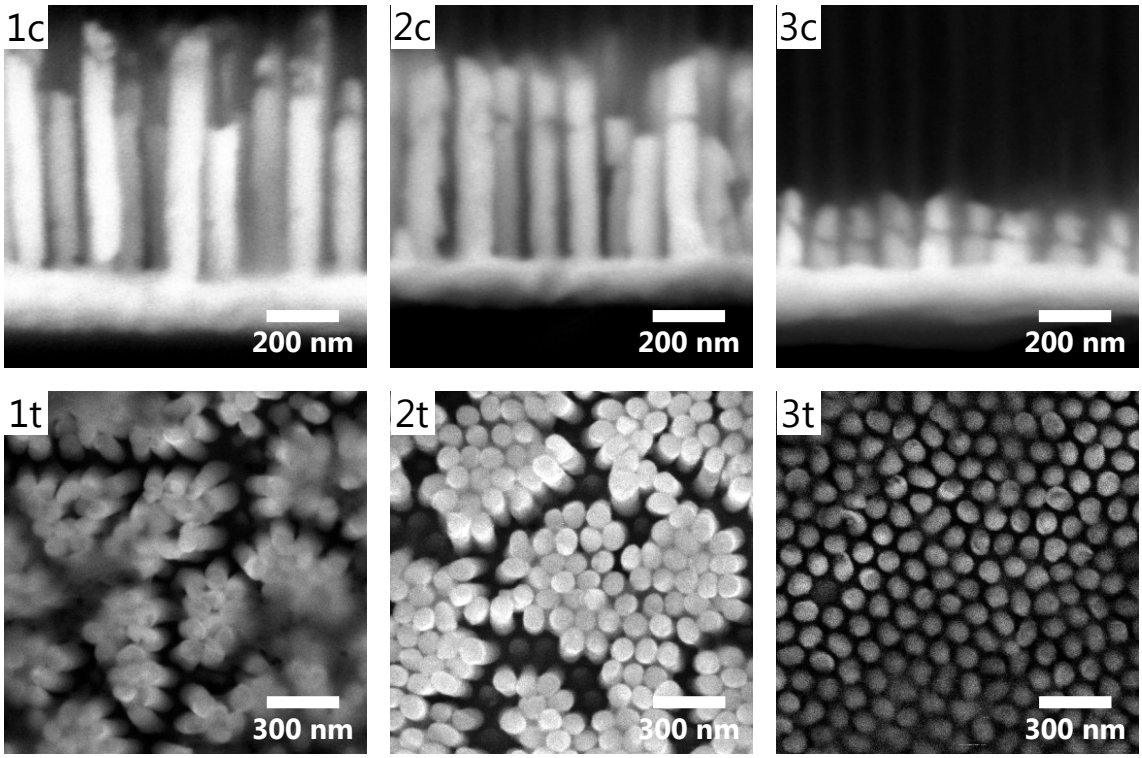

Fig. 4.6: The SEM images of Au-PANI-Au nanowires: cross section (c) and top view after removal of PAA (t). (1): Au, 1 $mAcm^{-2}$, 300 s; PANI, 1 $mAcm^{-2}$, 100 s; Au, 1 $mAcm^{-2}$, (100 s). (2): Au, 2 $mAcm^{-2}$, 150 s; PANI, 1 $mAcm^{-2}$, 30 s; Au, 2 $mAcm^{-2}$, 100 s. (3): Au, 2.5 $mAcm^{-2}$, 30 s; PANI, 2.5 $mAcm^{-2}$, 30 s; Au, 2.5 $mAcm^{-2}$, 30 s.

PANI layer is not very homogeneous and gold forms a shell-like structure around it. A similar behaviour of material penetration into PANI was proposed in the work [48] where authors suggested to postpone the next deposition on the PANI layer by at least 12 h. However, in this work, we deposited all segments sequentially and no time dependence studies were done.

We also studied the potentiostatic and galvanostatic deposition of gold. We found out that deposition at a higher current density over 5 $mAcm^{-2}$ or a voltage of 2.5 V, leads to etching of PAA accompanied by the evolution of bubbles during the process. Thus, all depositions were done using the current density of 0.5–2.5 $mAcm^{-2}$ or a voltage of 2 V. In both cases, the homogeneity of the final coverage highly depends on the electrolyte stirring. It was found that gentle or no stirring results in a macroscopically homogeneous coverage. Also slightly better coverage results were obtained from the potentiostatic deposition, although the SEM characterization did not show any differences.

Additionally, the deposition of gold from the non-cyanide bath (0.025M $HAuCl_4$, 0.42M Na_2SO_3, 0.42M $Na_2S_2O_3$) was briefly studied with the intention to avoid

using toxic cyanide solution, however it resulted in very inhomogeneous PAA filling.

4.2.4 Au-Ni-Au nanowires

Before we were able to obtain the desired results from the Au-PANI-Au deposition, we have focused on the nickel deposition as a substitution for PANI. The deposition of nickel has few advantages in respect to the PANI deposition. The main one is that nickel is reduced on the cathode while aniline has to undertake oxidation on the anode to be polymerized. This is directly connected with the choice of the substrate material. The substrate on which the PANI is deposited should not react during oxidation process. This excludes the majority of common materials (e.g.: Ni, Cu, Fe, Si). In this work, we unsuccessfully tried the deposition of PANI on the nickel nanowires and the copper substrate. Moreover, the electrochemical deposition of nickel results in a relatively compact microstructure while the polymerization can lead to various architectures (chains, networks).

Several representative results of Au-Ni-Au nanowires are shown in Figure 4.7 and characterized in Table 4.1. Here, we try to demonstrate the possibilities and limits of this technique. The smallest obtained segment length was 15 nm. However, the limiting factor is the SEM resolution, not the deposition parameters.

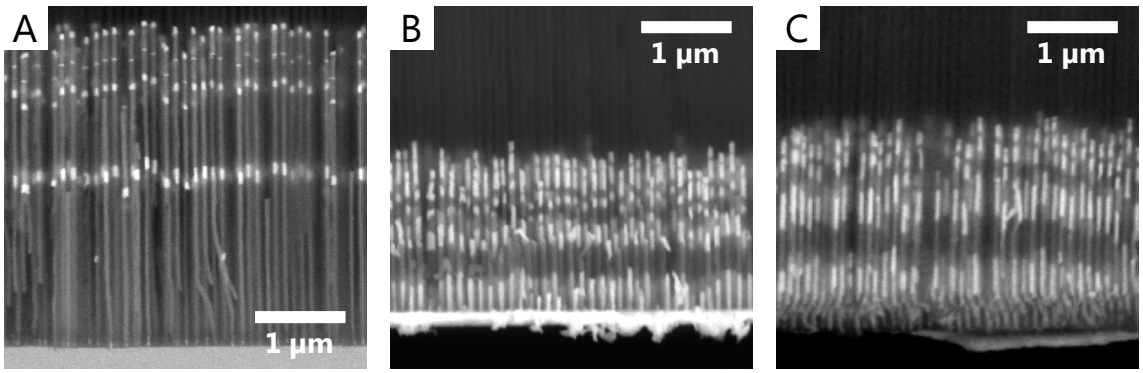

Fig. 4.7: The SEM images (cross section) of the Au-Ni-Au nanowires. The measured lengths of the segments are in Table 4.1.

As can be seen in Figure 4.7, deposited nickel (the darker parts between bright gold parts) form very compact segments compared to PANI. However, in both cases, the desired structure Au-Ni-Au or Au-PANI-Au is still connected with the gold substrate layer. Because the aim was to prepare the free-standing structures, we proposed the following method to achieve this.

The principle behind the method consists of the fabrication of desired structures, terminated by parts which can be selectively etched. At first, we fabricated Au-Ni-Au-Ni-Au-Ni-Au structure within the PAA template. To remove the gold layer,

Tab. 4.1: The lengths of the nanowire segments compared to their deposition time. The depositions of nickel (gold) resulted in the nanowires shown in Figure 4.7A, B, and C, and were done at 18 $mAcm^{-2}$ (1.8 $mAcm^{-2}$), 2.5 $mAcm^{-2}$ (2.5 $mAcm^{-2}$), and 1.2 $mAcm^{-2}$ (1.2 $mAcm^{-2}$), respectively.

segment of nanowire		Au	Ni	Au	Ni	Au	Ni	Au	Ni	Au
Figure 4.7A	time (s)		60	60	30	40	10	20	30	30
	length (nm)		1800	140	835	73	251	18	250	70
Figure 4.7B	time (s)	153	120	100	60	50	30	100	10	50
	length (nm)	340	360	230	180	86	94	190	22	107
Figure 4.7C	time (s)	300	300	150	150	75	50	47	17	30
	length (nm)	430	434	370	215	150	49	105	23	35

the sample was immersed for a few minutes into nickel compatible gold etchant, purchased from Sigma-Aldrich Co. LLC. The results are shown in Figure 4.8. The next step would be the selective etching of the nickel parts, however a solution which would selectively etch only nickel in respect to gold, was not found within this work. Therefore, we propose to substitute the terminating nickel part by copper. We

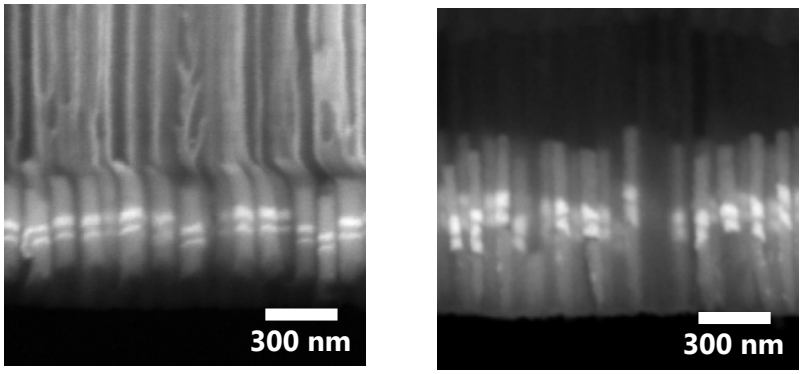

Fig. 4.8: The SEM images (cross section) of free-standing multi-layer structures within the PAA template. The sample (left) was prepared by deposition (Au, Ni) at 1.7 $mAcm^{-2}$: Au 100 s, Ni 150 s, Au 20 s, Ni 40 s, Au 20 s, Ni 154 s. The sample (right) was prepared by deposition (Au, Ni) at 2 $mAcm^{-2}$: Ni 100 s, Au 30 s, Ni 10 s, Au 30 s, Ni 100 s. The segments' (Au-Ni-Au) length is approximately 25 nm, 25 nm, 30 nm and 55 nm, 15 nm, 55 nm for image on the left and right, respectively.

experimentally confirmed the etching compatibility of the gold etchant with copper. Thus, before and after deposition of the desired structures, the copper part has to be deposited (e.g., Cu-Au-PANI-Au-Cu). The gold layer can be dissolved in the gold etchant while copper segments subsequently in a hydrochloric acid (HCl)

solution. The etching in HCl should not affect either gold, nickel, PANI or PAA. Unfortunately, due to time constraints only the deposition of these structures have been carried out while we plan to do selective etching experiments in the near future. The deposition of copper was done at a current density of $4\,\mathrm{mAcm^{-2}}$ or a voltage of 1 V for at least 30 s.

4.2.5 Chromium and silver deposition

In addition to the to previous experiments, we performed depositions of chromium nanowires (Figure 4.9Cr) and unsuccessfully tried to substitute the gold part by silver (Figure 4.9Ag). The chromium deposition resulted in a large length dispersion; probably caused by non-optimized deposition conditions. Later it was found that standard conditions for chromium electroplating are an increased temperature (40 °C) and a high current density ($300\,\mathrm{mAcm^{-2}}$). Moreover, we found out that our silver electrolyte (0.05M $AgNO_3$, 0.3M H_3BO_3) is probably not suitable for homogeneous nanowire deposition. This assumption is based on the work [49] where the authors clearly state that concentration of silver ions have to be as high as possible and the presence of nitrate ions is unacceptable.

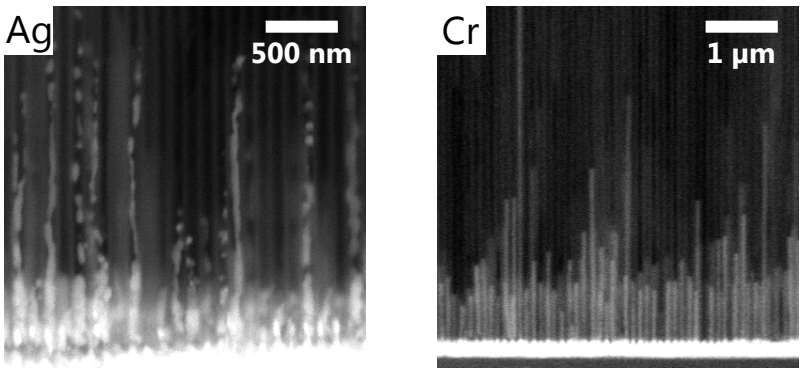

Fig. 4.9: The SEM images of the deposited Ag-Ni-Ag (Ag) and chromium (Cr) nanowires. Chromium was deposited by current density $200\,\mathrm{mAcm^{-2}}$ for 300 s. The unsuccessful deposition of the Ag-Ni-Ag nanowires were done at current density $1.4\,\mathrm{mAcm^{-2}}$: Ag 60 s, Ni 30 s, Ag 90 s.

At the end of this section, it is necessary to mention that no precise chemical characterization of the deposited material was done. Thus, it is not certain that the deposited nickel nanowires are composed of pure nickel and not other possible components (e.g.: nickel hydride, nickel oxide). The same is true for copper, chromium and PANI. In the case of gold and silver, the probability of obtaining pure materials is much greater based on the low chemical reactivity of gold and silver to form oxides, etc.

4.3 Calculations

To conclude this chapter, we will briefly discuss the empiric and theoretical approaches. In general, it is possible to calculate the length of deposited nanowires from the knowledge of transferred charge. However, a lot of empirical parameters are required: reaction efficiency, template porosity, etc. Here, we will demonstrate an illustrative calculation of reaction (current) efficiency based on experimental data (Figure 4.7). The aim is to point out the error in calculated results that originates in the measurement errors.

Based on the equation 1.6, we can write the following equation for theoretical current:

$$I_{\text{deposition}} = \mathrm{eN_A}zt\frac{m}{M}, \tag{4.1}$$

where the mass of deposited material m can be expressed as:

$$m = \rho\left(\alpha AL\right). \tag{4.2}$$

ρ is the density of the deposited material, α is the porosity of the PAA template, A is the area of PAA within which the material is the deposited and L is the length of deposited nanowires. Then the current efficiency can be expressed as:

$$\eta = \frac{I_{\text{deposition}}}{I_{\text{total}}}, \tag{4.3}$$

where $I_{\text{deposition}}$ is the theoretically calculated current accompanied by the deposition of material and I_{total} is the total measured current of the experiment (faradaic and nonfaradaic currents).

The calculated current efficiencies for various depositions including measurement errors are shown in Figure 4.10. Due to the simplified mass calculation, where we assumed the perfect cylindrical shape of nanowires with density of pure material, the current efficiencies are shifted to higher values. As seen in Figure 4.10, the current efficiency for gold and nickel is close to 30 % and 100 %, respectively. This low efficiency of the gold deposition is given by the high stability of the gold cyanide complex. On the other hand, the high efficiency of nickel is given by the high stability of free nickel cations. Moreover, the concentration of the nickel cations is approximately 60-times greater than the concentration of gold cations.

Due to the large measurement errors, the estimation of nanowire length has never been our aim. However, in precise systems with a well defined deposition area, calculations of this type are powerful tools to achieve fine control of the deposited nanowires.

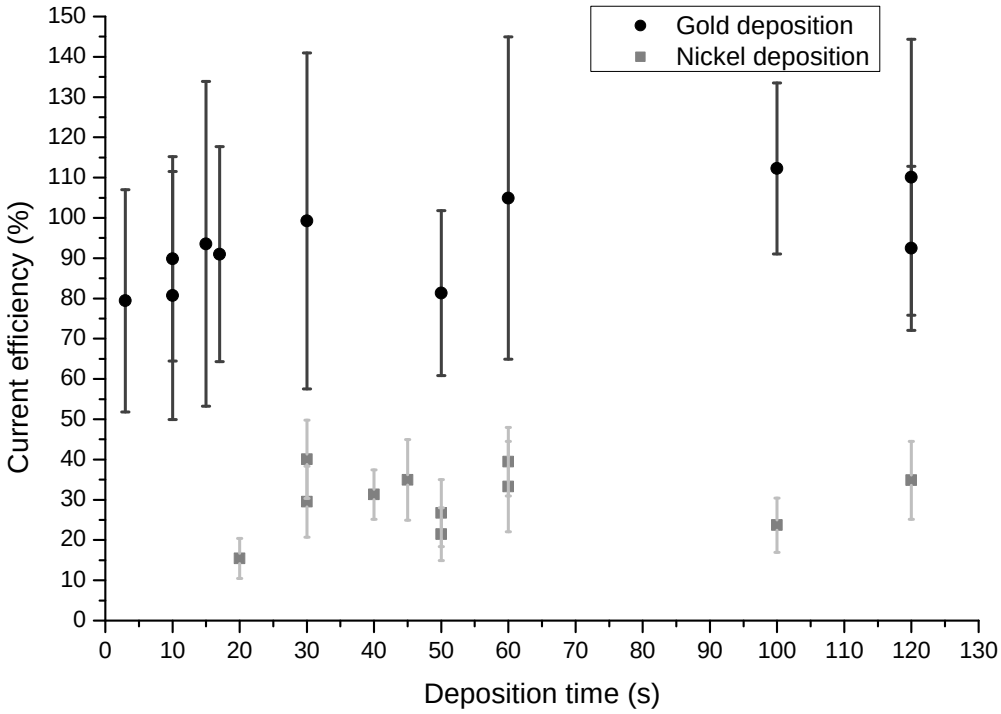

Fig. 4.10: The graph of the current efficiency relationship of various depositions represented by deposition time.

CONCLUSION

This work focused on the electrochemical deposition of multi-segment nanowires within the porous anodic alumina templates. The main goal was to fabricate the Au-PANI-Au structure of nanowires.

In chapter 1 we have introduced the basic principles of the electrochemistry in respect to the electrochemical deposition of metals as well as the polymerization of polyaniline. Chapter 2 is dedicated to porous anodic alumina (PAA), its characterization and the process of its formation. The practical part begins from chapter 3, where we have thoroughly described the fabrication process of the templates consisting of the preparation of the starting material, the anodization, and the modification of PAA. In chapter 4, we have discussed the selected methods and described the achieved results of the electrochemical deposition.

The major part of the practical work has been done in the laboratory of Microsensors and Nanotechnologies – LabSensNano (Department of Microelectronics, FEEC, BUT). A few minor procedures have been done in the laboratories and mechanical atelier of the Institute of Physical Engineering (FME, BUT) and in the laboratories of the Institute of Materials Science and Engineering (FME, BUT).

We have presented the mass fabrication of PAA templates with a highly-ordered pore structure and a pore diameter of approximately 50 nm. To improve the quality of the deposited gold layer, we have developed the annealing process leading to the remarkable results. The observed behaviour of the gold layer during the annealing process has led to the development of the novel technique for the large-scale production of a highly-ordered array of gold nanoparticles.

The PAA templates have been subsequently used for the preparation of the nanowires by electrochemical deposition. By this method, we have obtained the array of nanowires with the desired Au-PANI-Au structure. Moreover, we demonstrated that the substitution of PANI by nickel results in well-defined structures. These results (the SEM characterization and the deposition parameters) have been used for the illustrative calculation of the reaction efficiency. Additionally, we have studied the template assisted electrochemical deposition of silver, chromium and copper. While we have been able to obtain the free-standing Au-PANI-Au nanowires on the gold substrate layer, we proposed a method for the separation of these nanowires from the substrate.

Due to an absence of basic research and practical experience in this field, we have chosen the methods leading directly towards our goal. We have demonstrated the capability of these methods (anodization and electrochemical deposition) to prepare the desired nanostructures. We have deliberately avoided extensive empirical measurements which could result in the solving of time-consuming problems related

to measurements instead of the fabrication. Thus, it is believed that the chosen approach was the best solution which resulted in the successful achievement of our objectives.

For further work it would be interesting to study the properties (optical, electrical) of the formed nanowires within the PAA templates, as a free-standing array on a substrate or randomly distributed. The most attractive might be the dependence on the properties of PANI conductive-nonconductive state. Additionally, a significant work can be done to optimize the proposed deposition methods as well as the anodization of aluminium. However, at this time the most interesting appears to be the simple fabrication process of the gold nanoparticles array. To our knowledge, this technique has not been published yet, thus possible applications are still waiting to be discovered.

A SCANNING ELECTRON MICROSCOPY

In this chapter, we briefly discuss scanning electron microscopy or the scanning electron microscope (SEM). Despite this field providing enormous opportunities and possibilities of measurement, in this work we used only the basic techniques, thus the focus is on the description of the fundamental processes and function of the microscope in respect to the measured images.

In this work, we mainly used SEM MIRA2 and occasionally the LYRA3 from Tescan Orsay Holding, a.s. in the laboratories of LabSensNano (Department of Microelectronics, FEEC, BUT). Both microscopes are equipped with a standard detector of secondary electrons (SE) and a detector of back-scattered electrons (BSE). The MIRA2 is additionally equipped with the In-Beam SE detector which is a high efficiency SE detector placed in the objective lens (shown in Figure A.1).

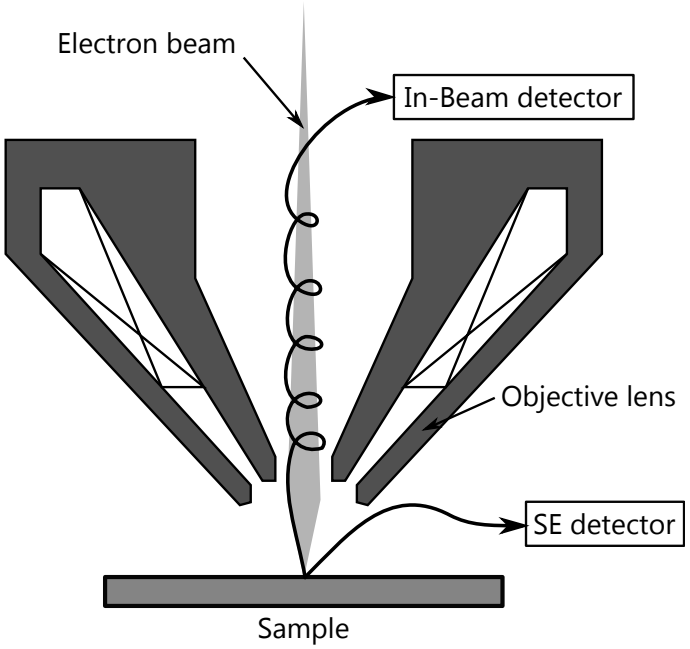

Fig. A.1: Schematic illustration of the standard SE detector compared to the In-Beam detector. (According to [50].)

The SE are generated mainly from the sample by the primary electrons of the beam. Because of their low energies (less than 50 eV), they are easily influenced by an electric field. This is used for detection: the positive potential on the detector grid is used to attract SE. However, the drawback is a large influence of the electrically charged samples on the measured images. This effect is most common in case of insulators (PAA, PMMA, etc.) or badly grounded samples and results in contrast and shape defects of the signal image. This behaviour is partially removed using the

In-Beam SE detector, where the SE have trajectories perpendicular to the sample (Figure A.1).

The most important result obtained is the information on the sample morphology given by the SE signal. The final signal is given not only by the generation of SE but also by the scattering events which occur during the electron's travel to a detector. As mentioned, the additional electric fields can deflect the electrons, thus less or more signal is detected. Also, important is the role of surrounding material which can absorb the electrons. This is nicely illustrated on the aluminium surface with hexagonally ordered pits shown in Figure 3.6. Here, the bottom of pit appears darker than the pit's edges, which is given by the absorption of the generated SE in the pits by the material of the edges. Additionally, the edges are higher placed, thus the generated SE can be easily detected. Moreover, the information depth of SE is only few nanometres. Despite the fact that the beam interaction volume is much larger in respect to the spot size, the SE carries only surface information. This is illustrated in Figure A.2.

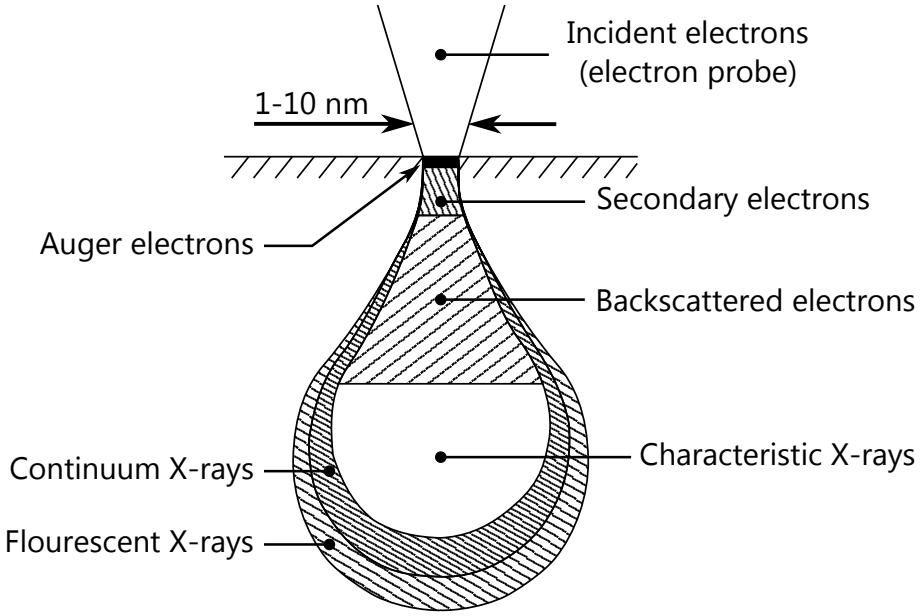

Fig. A.2: Schematic overview of the pear-shaped volume inside probed by different micropobe signals (electron and X-ray emission), when a primary electron beam is incident on a solid surface. (According to [51].)

For the nanowire characterization (exclude PANI nanowires), we used the detection of the BSE. The BSE are incident electrons which were elastically or inelastically scattered on the nuclei. Through this process we can obtain a good material contrast where heavy atoms (e.g., Au) appear brighter than lighter ones (e.g.: Al, Ni). Additionally, this technique is not significantly influenced by the sample charging

because of the high energies of the BSE (illustrated in Figure A.3). The disadvantage is a lower resolution compared to the SE due to the larger interaction volume.

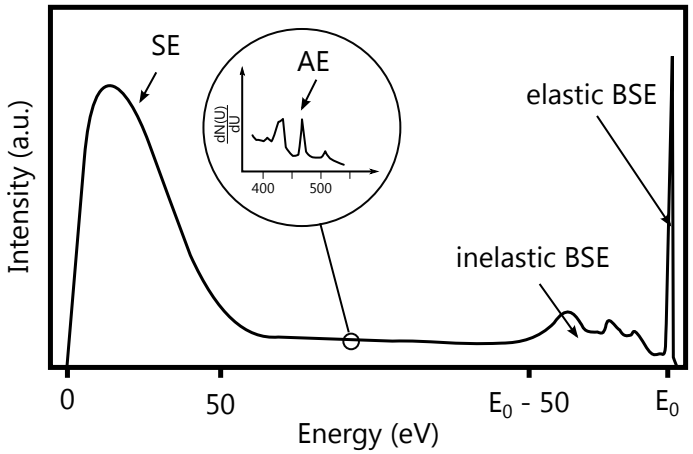

Fig. A.3: Qualitative large-scale overview of the energy distribution of electrons emitted from a surface which is irradiated by an electron beam of primary energy E_0. (According to [51].)

The measurement of length was done manually in the SEM software. This and the resolution of the acquired image are the main causes of the length measurement error. The error was estimated for structures of length over 500 nm to be 5 % while in case of the structures close to 20 nm it is over 30 %. In this work, the presented values are the average values of several measurements (more than 10).

BIBLIOGRAPHY

[1] Y. Xia, P. Yang, Y. Sun, Y. Wu, B. Mayers, B. Gates, Y. Yin, F. Kim, and H. Yan, "One-dimensional nanostructures: Synthesis, characterization, and applications," *Advanced Materials*, vol. 15, no. 5, pp. 353–389, 2003.

[2] M. T. Sheldon and H. A. Atwater, "The plasmoelectric effect: optically induced electrochemical potentials in resonant metallic structures," *ArXiv e-prints*, 2012.

[3] D. M. O'Carroll, J. S. Fakonas, D. M. Callahan, M. Schierhorn, and H. A. Atwater, "Metal–Polymer–Metal split-dipole nanoantennas," *Advanced Materials*, vol. 24, no. 23, pp. OP136–OP142, 2012.

[4] J. S. Tresback, A. Vasiliev, N. Padture, S.-Y. Park, and P. Berger, "Characterization and electrical properties of individual Au–NiO–Au heterojunction nanowires," *IEEE Transactions on Nanotechnology*, vol. 6, no. 6, pp. 676–681, 2007.

[5] D. Perego, S. Franz, M. Bestetti, L. Cattaneo, S. Brivio, G. Tallarida, and S. Spiga, "Engineered fabrication of ordered arrays of Au–NiO–Au nanowires," *Nanotechnology*, vol. 24, no. 4, p. 045302, 2013.

[6] V. S. Bagotsky, *Fundamentals of Electrochemistry: Electric Currents in Ionic Conductors*, 2nd ed. Wiley, 2005, pp. 1–18.

[7] A. Bard and L. Faulkner, *Electrochemical Methods: Fundamentals and Applications*, 2nd ed. Wiley, 2000.

[8] M. Staňo, "Fabrication of nanowires into porous alumina by electrolysis," Bachelor thesis (in czech), Brno University of Technology, Faculty of Mechanical Engineering, Brno, 2012.

[9] R. G. Ehl and A. J. Ihde, "Faraday's electrochemical laws and the determination of equivalent weights," *Journal of Chemical Education*, vol. 31, no. 5, p. 226, 1954.

[10] R. Calavia, A. Mozalev, R. Vazquez, I. Gracia, C. Cané, R. Ionescu, and E. Llobet, "Fabrication of WO_3 nanodot-based microsensors highly sensitive to hydrogen," *Sensors and Actuators B: Chemical*, vol. 149, no. 2, pp. 352–361, 2010.

[11] Y.-H. Chang, H.-W. Lin, and C. Chen, "Ultrafast initial growth rate of self-assembled TiO_2 nanorod arrays fabricated by Ti anodization," *Electrochemical and Solid-State Letters*, vol. 14, no. 1, pp. K1–K4, 2011.

[12] P. A. Kohl, *Electrodeposition of Gold*, 5th ed. John Wiley & Sons, Inc., 2010, pp. 115–130.

[13] S. Srinivasan, "Electrode/electrolyte interfaces: Structure and kinetics of charge transfer," in *Fuel Cells*. Springer US, 2006, pp. 27–92.

[14] P. Wilkinson, "Understanding gold plating," *Gold Bulletin*, vol. 19, no. 3, pp. 75–81, 1986.

[15] N. Gospodinova and L. Terlemezyan, "Conducting polymers prepared by oxidative polymerization: polyaniline," *Progress in Polymer Science*, vol. 23, no. 8, pp. 1443–1484, 1998.

[16] J. Stejskal, J. Prokeš, and M. Trchová, "Reprotonated polyanilines: The stability of conductivity at elevated temperature," *Polymer Degradation and Stability*, vol. 102, pp. 67–73, 2014.

[17] G. D. Sulka, *Highly Ordered Anodic Porous Alumina Formation by Self-Organized Anodizing*. Wiley-VCH Verlag GmbH & Co. KGaA, 2008, ch. 1, pp. 1–116.

[18] G. D. Bengough and J. M. Stuart, "Improved process of protecting surfaces of aluminium of aluminium alloys," United Kingdom Patent 223 994(A), 1923.

[19] J. W. Diggle, T. C. Downie, and C. W. Goulding, "Anodic oxide films on aluminum," *Chemical Reviews*, vol. 69, no. 3, pp. 365–405, 1969.

[20] G. E. Thompson, "Porous anodic alumina: fabrication, characterization and applications," *Thin Solid Films*, vol. 297, no. 1-2, pp. 192–201, 1997.

[21] F. Keller, M. S. Hunter, and D. L. Robinson, "Structural features of oxide coatings on aluminum," *Journal of The Electrochemical Society*, vol. 100, no. 9, pp. 411–419, 1953.

[22] H. Masuda and K. Fukuda, "Ordered metal nanohole arrays made by a two-step replication of honeycomb structures of anodic alumina," *Science*, vol. 268, no. 5216, pp. 1466–1468, 1995.

[23] H. Masuda and M. Satoh, "Fabrication of gold nanodot array using anodic porous alumina as an evaporation mask," *Japanese Journal of Applied Physics*, vol. 35, no. Part 2, No. 1B, pp. L126–L129, 1996.

[24] T. P. Hoar and J. Yahalom, "The initiation of pores in anodic oxide films formed on aluminum in acid solutions," *Journal of The Electrochemical Society*, vol. 110, no. 6, pp. 614–621, 1963.

[25] H. Masuda, H. Asoh, M. Watanabe, K. Nishio, M. Nakao, and T. Tamamura, "Square and triangular nanohole array architectures in anodic alumina," *Advanced Materials*, vol. 13, no. 3, pp. 189–192, 2001.

[26] Z. Su and W. Zhou, "Porous anodic metal oxides," *Science Foundation in China*, vol. 16, no. 1, p. 36, 2008.

[27] L. Vojkůvka, L. Marsal, J. Ferré-Borrull, P. Formentin, and J. Pallarès, "Self-ordered porous alumina membranes with large lattice constant fabricated by hard anodization," *Superlattices and Microstructures*, vol. 44, no. 45, pp. 577–582, 2008.

[28] Y. Li, Z. Y. Ling, S. S. Chen, and J. C. Wang, "Fabrication of novel porous anodic alumina membranes by two-step hard anodization," *Nanotechnology*, vol. 19, no. 22, p. 225604, 2008.

[29] A. Thormann, N. Teuscher, M. Pfannmöller, U. Rothe, and A. Heilmann, "Nanoporous aluminum oxide membranes for filtration and biofunctionalization," *Small*, vol. 3, no. 6, pp. 1032–1040, 2007.

[30] Z. Král, L. Vojkůvka, E. Garcia-Caurel, J. Ferré-Borrull, L. F. Marsal, and J. Pallarès, "Calculation of angular-dependent reflectance and polarimetry spectra of nanoporous anodic alumina-based photonic crystal slabs," *Photonics and Nanostructures - Fundamentals and Applications*, vol. 7, no. 1, pp. 12–18, 2009.

[31] S. Shingubara, "Fabrication of nanomaterials using porous alumina templates," *Journal of Nanoparticle Research*, vol. 5, no. 1-2, pp. 17–30, 2003.

[32] A. Ramazani, M. A. Kashi, and G. Seyedi, "Crystallinity and magnetic properties of electrodeposited Co nanowires in porous alumina," *Journal of Magnetism and Magnetic Materials*, vol. 324, no. 10, pp. 1826–1831, 2012.

[33] W. Lee, R. Ji, U. Gösele, and K. Nielsch, "Fast fabrication of long-range ordered porous alumina membranes by hard anodization," *Nature Materials*, vol. 5, no. 9, pp. 741–747, 2006.

[34] S. Ono, M. Saito, M. Ishiguro, and H. Asoh, "Controlling factor of self-ordering of anodic porous alumina," *Journal of The Electrochemical Society*, vol. 151, no. 8, pp. B473–B478, 2004.

[35] P. Erdogan and Y. Birol, "Effect of processing on structural features of anodic aluminum oxides," *Applied Physics A*, vol. 108, no. 3, pp. 587–592, 2012.

[36] L. Zaraska, W. J. Stępniowski, E. Ciepiela, and G. D. Sulka, "The effect of anodizing temperature on structural features and hexagonal arrangement of nanopores in alumina synthesized by two-step anodizing in oxalic acid," *Thin Solid Films*, vol. 534, pp. 155–161, 2013.

[37] A. Santos, L. Vojkůvka, J. Pallarès, J. Ferré-Borrull, and L. Marsal, "In situ electrochemical dissolution of the oxide barrier layer of porous anodic alumina fabricated by hard anodization," *Journal of Electroanalytical Chemistry*, vol. 632, no. 1–2, pp. 139–142, 2009.

[38] K. Ersching, E. Dorico, R. da Silva, V. Zoldan, E. Isoppo, A. Viegas, and A. Pasa, "Surface and interface characterization of nanoporous alumina templates produced in oxalic acid and submitted to etching procedures," *Materials Chemistry and Physics*, vol. 137, no. 1, pp. 140–146, 2012.

[39] G. Sharma, M. V. Pishko, and C. A. Grimes, "Fabrication of metallic nanowire arrays by electrodeposition into nanoporous alumina membranes: effect of barrier layer," *Journal of Materials Science*, vol. 42, no. 13, pp. 4738–4744, 2007.

[40] S. Zhao, K. Chan, A. Yelon, and T. Veres, "Preparation of open-through anodized aluminium oxide films with a clean method," *Nanotechnology*, vol. 18, no. 24, p. 245304, 2007.

[41] J. Yuan, W. Chen, R. Hui, Y. Hu, and X. Xia, "Mechanism of one-step voltage pulse detachment of porous anodic alumina membranes," *Electrochimica Acta*, vol. 51, no. 22, pp. 4589–4595, 2006.

[42] T. Lednický, "Fabrication and characterization of the templates for fabrication of nanowires," Bachelor thesis (in czech), Brno University of Technology, Faculty of Mechanical Engineering, Brno, 2012.

[43] C. M. Müller and R. Spolenak, "Microstructure evolution during dewetting in thin Au films," *Acta Materialia*, vol. 58, no. 18, pp. 6035–6045, 2010.

[44] C. Worsch, M. Kracker, W. Wisniewski, and C. Rüssel, "Optical properties of self assembled oriented island evolution of ultra-thin gold layers," *Thin Solid Films*, vol. 520, no. 15, pp. 4941–4946, 2012.

[45] A. Mozalev, V. Khatko, C. Bittencourt, A. W. Hassel, G. Gorokh, E. Llobet, and X. Correig, "Nanostructured columnlike tungsten oxide film by anodizing Al/W/Ti layers on Si," *Chemistry of Materials*, vol. 20, no. 20, pp. 6482–6493, 2008.

[46] M. J. Liew, S. Roy, and K. Scott, "Development of a non-toxic electrolyte for soft gold electrodeposition: an overview of work at University of Newcastle upon Tyne," *Green Chemistry*, vol. 5, pp. 376–381, 2003.

[47] M. L. Chourou, K. Fukami, T. Sakka, and Y. H. Ogata, "Gold electrodeposition into porous silicon: Comparison between meso- and macroporous silicon," *physica status solidi (c)*, vol. 8, no. 6, pp. 1783–1786, 2011.

[48] T. Sehayek, D. Meisel, A. Vaskevich, and I. Rubinstein, "Laterally controlled template electrodeposition of polyaniline," *Israel Journal of Chemistry*, vol. 48, no. 3-4, pp. 359–366, 2008.

[49] G. Sauer, G. Brehm, S. Schneider, K. Nielsch, R. B. Wehrspohn, J. Choi, H. Hofmeister, and U. Gösele, "Highly ordered monocrystalline silver nanowire arrays," *Journal of Applied Physics*, vol. 91, no. 5, pp. 3243–3247, 2002.

[50] W. Zhou, R. Apkarian, Z. Wang, and D. Joy, "Fundamentals of scanning electron microscopy (SEM)," in *Scanning Microscopy for Nanotechnology*, W. Zhou and Z. Wang, Eds. Springer New York, 2007, pp. 1–40.

[51] H. Lüth, "Morphology and structure of surfaces, interfaces and thin films," in *Solid Surfaces, Interfaces and Thin Films*, ser. Graduate Texts in Physics. Springer Berlin Heidelberg, 2010, pp. 67–131.